2006

Insights to the character and possible seasonal evolution of the subglacial drainage system of the Matanuska Glacier, Alaska; as determined by dye injection experiments

James J. Cascione
Lehigh University

Cascione, James J.

Insights to the Character and Possible Seasonal Evolution of the Subglacial Drainage...

January 2006

Insights to the Character and Possible Seasonal Evolution of the Subglacial Drainage System of the Matanuska Glacier, Alaska; as Determined by Dye Injection Experiments

By

James J. Cascione

A Thesis

Presented to the Graduate and Research Committee

of Lehigh University

in Candidacy for the Degree of

Master of Science

In

Department of Earth and Environmental Sciences

Lehigh University

December, 2005

This thesis is accepted and approved in partial fulfillment of the requirements for the Master of Science.

12/08/05
Date

Approved by:

Dr. Edward Evenson
(Thesis Advisor)

Dr. Peter Zietler
(Chairperson of Department)

Acknowledgements

I would like to thank Dr. Ed Evenson for his continued support, guidance, and most importantly the friendship that he has given for these past many years. I would like to thank Dr. Dan Lawson whose support and resources were invaluable to my research and development of my thesis. I would like to thank Dr. Grahame Larson and Dr. Gerard Lennon whose insights were most helpful in formulating my work. Without the help of many people in the field my research would not have been possible, especially Bill Stevenson, Nick Waterson, Evan Mankoff, and Todd Johnston. I would also like to thank the grad community here at Lehigh for help in solving the hundreds of problems that so often arise, especially Karina Walker, to whom I am forever indebted.

Table of Contents

List of Figures

List of Tables

List of Appendices

Insights to the Character and Possible Seasonal Evolution of the Subglacial Drainage System of the Matanuska Glacier, Alaska; as Determined by Dye Injection Experiments

Abstract

In this thesis, I present data from dye injection experiments within the subglacial drainage system of the Matanuska Glacier of south-central Alaska conducted to investigate the extent and conditions of water flow along the glacier's bed during the course of the 2002 summer melt season. Twelve injections of Rhodamine WT dye into boreholes was done at four sites within one kilometer of the glacier's terminus. The dye within the subglacial water exiting in terminal vents was collected both by adsorption on the surface of activated charcoal and discreet water sampling. My results show that dye would often flow through numerous subglacial pathways and exit from multiple vents across the terminus. Dye breakthrough curves were used to calculate varying metrics of the traveling dye cloud and to interpret drainage system geometry. Calculated average linear flow velocities varied order of magnitude from 0.014 to 0.380 m/s, highlighting probable differences in localized drainage configurations that can either constrict or route water quickly beneath the glacier. Dispersivity values calculated from the shape of the dye return curves ranged from 6.56m for fast-flowing, near terminus channels of the southern study area, to 115.8m for multiple constricted pathways within the northern study area. Additional field evidence and seasonal discharge records support drainage system evolution during the course of the melt season.

Based on the data from this study I suggest that the subglacial drainage system of the Matanuska Glacier is characterized by an early season, distributed network of unique

drainage pathways that expands and evolves during the course of the melt season. At the beginning of the melt season individual discharge vents may be serviced by a subglacial network that remains isolated from adjacent pathways. As meltwater inputs rise during the melt season the overall system expands and the localized segregation of drainage pathways lessens. Near terminus areas that maintained high basal water pressures and low velocities regardless of meltwater discharge decreases may signify the constriction of channels by the process of frazil ice growth within an overdeepening as reported by Lawson et al. (1998) and Alley et al. (1998).

Introduction

Surface water sources are generated from meteoric water, the melting of snow and ice on the glacial surface, and runoff from surrounding valley slopes during the summer months. Water flows over the glacial surface, in supraglacial streams until it either enters the internal drainage network through moulins and crevasses, or until it flows off of the glacier surface at the terminus. The subglacial drainage system transports the majority of the surface water input to exit points along the glacial terminus, here called 'vents' that feed proglacial streams.

Indirect methods, most notably using dye-tracer studies, have previously been used to develop different plausible configurations of the subglacial drainage system (Seaberg et al. 1988). Two distinct models of subglacial drainage systems have been developed. They are commonly referred to as "discrete drainage systems" and "distributed drainage systems". Discrete drainage systems move meltwater efficiently through channels that have been eroded into the underlying bed and/or incised in the overlying ice (Fig 1a, Hubbard et al., 1995). The stability of a channelized drainage network is controlled by the ability of the flowing water to maintain its local channel morphology, through frictional melting of the channel walls and the evacuation of sediment. Decreases in discharge will result in sediment deposition and the plastic deformation of the overlying ice, reducing the flow area of the channel.

In contrast, distributed drainage systems drain large areas at much lower flow rates via meltwater films at the ice bed interface, via linked cavities formed within bed

irregularities, and through permeable, subglacial sediments (Fig 1b, Hubbard, et al. 1995). Distributed systems are maintained at lower discharge rates due to the greater control of bed composition and/or morphology and the lower frictional melting or erosional power of the flowing water.

The interaction, co-existence, and evolution of these two subglacial drainage configurations is a function of the flux of basal melt water, the rate of melting of channel walls by the heat of viscous dissipation of flowing water and the rate of ice deformation and subsequent closure of the conduits. Dye-tracer studies of the Haut Glacier d'Arolla provide evidence that a subglacial drainage configuration can undergo evolution, over the course of the melt season, from a distributed system, maintained during winter months by very low discharges of basal water, to channelized drainage as melt water volumes increase and melting enlarges conduits along preferred flow-paths (Nienow et al., 1998).

Glaciers often erode basins (called "overdeepenings") within their beds, and water traveling out of these basins must rise in the direction of ice flow, while ice surface slope may remain constant (Alley et al. 1998). The rise of the subglacial water over the adverse slope of the overdeepening can lead to supercooled water, as the pressure-melting point rises with limited heating by viscous dissipation (Lawson et al., 1998; Hooke and Pohjola, 1994). Rapid ice crystal nucleation and growth may result along the conduit walls, restricting the flow of water and diverting flow paths, thus forcing a distributed subglacial configuration (Lawson et al., 1998). If a subglacial drainage system is restricted by this process of supercooling and the growth of ice within conduits, the drainage configuration must evolve an alternate method to move the water being

delivered to the base of the glacier.

The object of this study is to investigate the relationship between the subglacial water flux and the drainage configuration's response, perhaps evolving over the melt season. Analyzing the results from dye injection experiments may also help to reveal the changes in basal water pressure and routing within the system during the melt season, providing insight to the timing, evolution and duration of the subglacial drainage system and the freeze-on mechanism.

Setting and Previous Study

The Matanuska Glacier is a large (approximately 45 km long) valley glacier that ends at a terminal lobe 5km wide (Fig. 2, Lawson et al. 1998). The study area is located on the western end of the terminal lobe where numerous vents along the ice margin release pressurized, subglacial water (Fig.3). During high discharge, upwellings of water are often visible on the stream surface that runs along the ice margin (Fig.3) indicating the exit points of the subglacial drainage network. A gaging station approximately 200m downstream of the glacier terminus (SGS, Fig. 3) records the combined discharge of all the vents along the western margin of the glacier. A second gauging station (LRV, Fig. 3) records the discharge of a single vent north of the main stream.

The western end of the Matanuska Glacier flows out of an ice marginal overdeepening, as evidenced by GPR profiles of the glacier bed (Arcone, 1995). Based on preliminary dye tracer experiments Lawson and others (1998) and Alley and others (1998) hypothesize that the subglacial system of the Matanuska Glacier is a distributed

configuration of low broad channels within the underlying subglacial sediment. An ubiquitous zone of debris-rich, isotopically young, basal ice is present along the exposed terminus of the Matanuska Glacier, typically ranging in thickness of 3 to 6 m (Lawson et al., 1998). The origin of this debris rich (typically 19 to 23% by volume) basal ice is hypothesized to be a product of glaciohydraulic supercooling within the subglacial drainage system. As water climbs the adverse slope of the overdeepening, sediment is entrained during ice growth in the supercooled water (Lawson et al., 1998; Alley et al. 1998). A widely distributed drainage system is necessary for extensive basal ice accretion, and formation of the basal zone ice.

Methods:

Dye tracing experiments have been utilized by numerous researchers for the characterization of flow within subglacial drainage system (e.g. Seaberg et al., 1988; Willis et al., 1990; Fountain, 1993; Kohler, 1995; Nienow et al., 1996; Lawson et al., 1998). Moulins are predominantly used as the input points for these dye tracing experiments since they are the natural entrance for meltwater to the subglacial system and a convenient "injection point" for dye tracer studies. However, the often complex structure of moulins is often ignored, oversimplified or not considered. Moulins are in actuality the entrance to the englacial drainage system which can be considered connected to, but separate from, the subglacial drainage system. The morphology of a "moulin - englacial conduit system" may be a simple "pipe like" pathway, or may include a complex series of plunge pools and meandering conduits following the orientation of the original crevasses and subsequent fractures (Seaberg et al., 1988). Directly accessing the subglacial meltwater system with boreholes, as was done in this study, removes the influence of the unknown englacial flow path and provides greater accuracy when attempting to characterize the subglacial system with dye tracers.

In this study, I accessed the subglacial drainage system for dye injection by melting boreholes to the glacier's bed using a Taylor Scientific Engineering drill system owned and operated by the USACE Cold Regions Research and Engineering Lab (CRREL). The high-pressure, hot-water drill introduces a 300KBTU/hr energy input to a 15cm diameter water filled hole, melting through temperate englacial ice at an average

rate of 1 meter per minute (Taylor, 1984). A direct connection with the subglacial drainage system was accomplished and recognized when the water-filled borehole "flushed". This rapid draining of the water column is due to the weight of the water in the borehole equalizing with the basal water pressures within the subglacial system. After a hole flushed, drilling continued until refusal of the drill stem to advance and the load measured on the drill tower had significantly decreased, indicating that the stem was being supported by the bed of the glacier. A total of nine boreholes were drilled during the course of the study. Five (BH2, BH5, BH6, BH8, BH9, Fig. 3) of these flushed and were used for dye injection. Selection of borehole locations was based on an attempt to maintain a straight line, in the down ice direction, between progressively closer boreholes and a selected vent. Thus the tracer test results could be compared to any differences in the organization of the drainage pathway as you move "down stream" within the theoretical subglacial "drainage basin".

The location of gaging stations, boreholes and ice marginal vents utilized in this study are shown in Figure 3. The most recent aerial photograph available (06/1997) was geo-referenced to a digital copy of the 1948 USGS topographic map (Anchorage quads D-3 and D-2) by anchoring points of observable geomorphic and anthropogenic features. The relative spatial relationship between boreholes and vents is accurate within an estimated 2m.

Rhodamine WT fluorescent dye was used as a tracer in this study. The selection of Rhodamine WT was based upon cost, the low detection limit, and previous successful use at the Matanuska and other glacial systems (eg. Lawson et al., 1998 ; Isaacs, 2001;

Hooke and Phojla, 1994; Hasnain et al., 2001).

The dye was injected at the base of the borehole by several methods. Initially, a container was engineered to release dye through the drill stem using the pressurized hot water stream. During the first three attempts, difficulties in the dye release valve assembly led to over-pressurization during injection and the total quantity of dye in the container was not injected in a single pulse. In addition, concerns of possible contamination from residual dye in the drill hose led me to develop of a simpler dye injection method – the "PVC injector". A 46cm section of 11cm diameter PVC pipe, capped and sealed on both ends, acted as a container for the dye. A small (3cm) opening was drilled at each end. One opening was fitted with a threaded connector and attached to the drill stem; the other end was sealed with a rubber cork. The PVC container was then lowered to the desired depth and the water pumps on the drill system were activated to push out the cork and release the dye in a near instantaneous pulse. Attempts to use the same approach but with compressed air at borehole BH6 (run #9) were unsuccessful, most likely due to the high water pressure at depth within the borehole and an air leak at the threaded coupling.

During run #5, when the drill was unavailable, manual injection was made by enclosing dye in a large, sealed Zip-loc bag. The Zip-loc bag was lowered on a cable to the desired depth and crushed by sending a weight down the cable. When the line was drawn up, the bag had been torn from the line as evidenced by only a corner of the bag remaining. I presume that the dye had been released at depth and the bag had been ripped apart during the ascent due through the narrow diameter borehole.

Dye was released into surface streams entering two moulins located within the vicinity of BH2 and BH8 (Fig. 3) to determine if englacial pathways result in an increase in the number of positive connections with ice-marginal vents compared to those identified by subglacial injections.

Charcoal Bug Sampling

The location(s) of the dye exiting from one or more ice-marginal vents after an injection was determined by the absorption of the dye on the surface of granular activated coconut carbon (referred to here, and in the literature, as "charcoal bugs") following procedures outlined in the EPA manual for dye tracing within karst terrains (Mull et al., 1988). The charcoal bugs, encased in nylon screening, were suspended within several vents during each test, additional bugs were deployed within ice-marginal streams near each vent to provide sampling redundancy in case the charcoal bugs was lost or destroyed in the high pressure discharge that was common to each vent. The bugs were deployed the morning of a dye injection and collected 48 hours after injection. Each bug was transferred to a sealed sample bag and brought to the field lab where they were washed to remove any silt or mud and dried overnight in an oven at 49 degree C. Three gram samples of the dried charcoal were placed in labeled plastic containers. Then, 45ml of eluent, consisting of 43% 1-proponal, 19% distilled water, and 38% ammonium hydroxide (28-30% assay) (Mull et al., 1988; Smart, 1972), was added to the charcoal subsample and each container was sealed and covered to avoid photochemical decay.

After one hour the elutant was transferred to borosilicate cuvettes and placed in a water bath and allowed to equilibrate to a temperature of 23.9 deg. C along with eluent blanks and dye concentration standards.

Samples were tested for dye concentration using a calibrated Turner Designs Model 10-AU filter fluorometer. Calibration standards for the fluorometer were created at the field station, following the dilution procedures outlined in Mull and others (1988). Dilution by mass was used in place of standard volume dilutions since volumetric flasks were not available. The density of water with Rhodamine WT dye concentrations of 100ppb and less was assumed to be 1 kg/L. A single set of standards with concentrations of 10ppb, 1ppb, and .1ppb and .01ppb were created with filtered Matanuska River water for calibrating of the fluorometer before testing each suite of samples (Wilson et al., 1986). Standards were stored in clean brown glass bottles capped and covered to prohibit photochemical decay. Control samples were taken during each experiment and subsequent sample testing. Each batch of eluent was tested before sample preparation; the batch was disregarded if a positive value for fluorescence was found. Control samples of dry charcoal washed with distilled water returned an average dye concentration of 0.008ppb ± 0.002ppb. The false values found from the distilled water control samples are thought to originate from charcoal fines that were not removed by filtration or settling. Additional charcoal samples were deployed within the north branch of the Matanuska River which is isolated from the discharge of study area. These control receptors consistently returned a positive fluorescence value, ranging from 0.014ppb to 0.032ppb with an average concentration of 0.021ppb ± 0.004ppb. The false positive readings are

thought to originate from some combination of charcoal fines, slit grains, and natural or anthropogenic compounds absorbed onto the charcoal that have similar emitting spectra as Rhodamine WT.

Due to the observed background fluorescence, semi-quantitative categories are used to characterize the relative strength of the vent to borehole connections determined by the charcoal samples. Concentration values below 0.025ppb are considered background and therefore "no connection" between vents and borehole. Values from 0.025ppb to 0.050ppb are considered "possible" connections since the values are above average background, yet are not significantly greater than the maximum background value. A value between 0.050ppb and 0.100ppb is considered "weak". A value greater than 0.100ppb is considered a "strong" connection.

Subglacial Water Sampling

Subglacial water was sampled using ISCO automated water samplers that were deployed prior to dye injection. The number of available ISCOs for the tracer tests varied during the field season and thus sampling had to be restricted to a single vent or several vents closest to the injection borehole in the down ice direction and that were thought to be the most likely to communicate subglacially with the test borehole. Initially sample rates (number of discreet samples collected per hour) were calculated from flow velocity data of from previous dye tracing studies (Lawson, 1998; Isaces, 2001; Burnett, 2001) but were adjusted during the course of the field season based on my results to better capture the exiting dye. During tracer tests with greatest straight-line distances (injections from

BH2 and BH9), water from the second to last ISCO collection bottle was tested for the presence of dye to determine whether additional sampling with the ISCO was needed to capture the entire dye cloud.

After transport of the ISCO bottles to the field station, sediment was allowed to settle within the collection bottles and then the water was filtered through clean glass fiber filters with grain size retention of 1.6μm to remove any additional suspended sediment prior to analysis. To reduce the chance of accidental cross contamination, each suite of samples was filtered in the order of presumed lowest to highest dye concentration that would result in a Gaussian shaped curve. Samples at the ends of the chronologically ordered suite were filtered first, while middle samples were filtered last. Collection flasks were rinsed with distilled water between samples. Filtered water samples were placed in labeled plastic bottles capped and covered to prevent photochemical decay. When all samples had been filtered, subsamples of water were transferred to labeled borosilicate cuvettes. These were placed within a water bath with additional fluorometer calibration standards and allowed to equilibrate to the testing temperature of 23.9 deg. C. To ensure consistent readings from the fluorometer between samples, an automated averaging function was employed (Wilson et al., 1986). This method allows a standard time delay before concentration values are recorded and then averages the recorded values over an additional time period. A default delay period of 15 seconds and an averaging period of 10 seconds were selected. Replicate testing of 3 to 4 random samples within each suite yielded an average error range of ± 0.002ppb.

Results:

Charcoal Bugs

Table 1 summarizes the results of the dye tracing tests using the charcoal bug indicators, listing the qualitatively determined borehole to vent connections made through the field season. Of the fourteen experiments attempted (runs 1-14, Table 1), nine resulted in absorption of sufficient dye to be considered "connections" and two as "possible connections". Figure 4 shows each borehole to vent connection during each dye runs. Strong connections between boreholes near the terminus (BH 5 & 6) and vents were found during early to mid-season tests. (run # 3, 5, 7, 8 and 10). Weaker connections were made from injection sites farther from the terminus (BH 2, 8, & 9) as well as later in the season from BH5 (run #14). Importantly, multiple vents were often found to connect along flow paths from single injection points (Fig. 4).

Dye Breakthrough Curves

Figures 5-19 are graphs of dye return values with an interpolated return curve constructed by applying a "Loess smoothing factor" which produced the best visual curve to the raw data. Smoothing and interpolating data between the discreet sampling intervals was necessary to extract values from a curve that is traditionally used in dye return curve analysis.

Discharge Records

Normalized discharge records from SGS (South Gauging Station) and Little River

gauging station are shown in Fig. 20 with the dates of successful injection experiments. The normalized values were calculated by dividing the 15min interval data by the highest discharge value recorded at each gauging station during the melt season. The values were then averaged over a three hour moving window to highlight the overall seasonal trend in each discharge record, while preserving the diurnal range that results from daily temperature, insolation, and precipitation fluctuations. Injection experiments connecting with LRV (Little River Vent, blue date lines on Fig. 20) were conducted within the general trend of decreasing discharge from an early melt season maximum while the overall system discharge (SGS) was increasing to a mid-season maximum. Relatively similar discharges are assumed to have exited the individual MEGA and MAM vents during the relatively steady, mid-season discharge recorded by SGS during July (red date lines on Fig. 20).

Discussion:

Charcoal Bugs

During the course of the melt season, single borehole injections repeatedly make connections with several vents (Fig. 4), indicating that subglacial flow spreads laterally and/or bifurcates in the down-ice direction toward the terminus. These data suggest that a "channelized dendritic network" (Fig. 1A), did not exist, since then, dye injected in a single pathway would be expected to funnel through increasingly efficient channels and exit out a single vent. All subsequent interpretations must be considered in the context of this simple, yet extremely important observation.

Experiments that were conducted closest to the terminus (BH5 and BH6) show restricted lateral spreading across the terminus. The exiting dye is limited to those vents located almost directly down ice from the injection borehole, indicating that the near terminus flow paths are effectively separated from one another and suggesting a "northern" and "southern" drainage basin exist (Fig. 21). Tracers injected in boreholes located up-glacier (BH2 and BH8) maintain this limited connectivity to vents directly down ice from the injection point, and further reinforcing the hypothesis of two drainage basins (Fig. 22). The absence of overlapping flow paths points suggests that a physical (higher bed elevation) or hydraulic separation between the northern and southern halves of the study area restricts drainage, though no surface expression of this separation is apparent from observation.

An expansion of the dye cloud occurs from an injection points farther from terminus within the southern drainage area (BH8), shown by run# 11 (red area, Fig. 22).

The evidence strengthens the argument for a distributed network of channels that would result in a greater number of flow paths delivering dye laterally across the terminus. The relationship does not exist within the northern drainage in an early season test (run #6) from BH2 (blue area, Fig 22) perhaps due to an initial lack of maturity of this drainage network at the time. Expansion of the northern drainage as the system matures is shown from the lateral extent of the dye cloud from run #7, a later repeat of run #3, showing additional borehole to vent connections had been established to the northern Little River vent (LRV, Fig 23). Further evidence of the seasonal evolution of the entire drainage system is shown by the mid-season injection from BH9 (the original location of the earlier drilled BH2) establishing connections across the study area, highlighting the loss of the spatial isolation between the northern and southern drainage areas (Fig. 24).

Taking the semi-qualitative dye values found from injections at BH5 we find further support for a seasonal evolution of the northern drainage network. Fig. 25 shows that during an early season test (run #5), the concentrations recorded at vents decrease as straight-line distances from the injection point increase. Decreasing dye concentrations can be expected as injection to vent distances increase in both distributed and channelized systems from the introduction of undyed "clean" water along the travel path of the dye cloud (Fig. 26). The mid-season run #7 from BH5 does not agree with this expected result, with a higher concentration found at the more distant LRV as compared to the POND vent (Fig. 27), suggesting that the initial connection to LRV had subsequently matured and the dye cloud now follows a preferred pathway to the more distant exiting vent. The late season test (Run #14), repeating the previous injections from BH5,

confirms the interpretation. The results show a contraction of borehole to vent connections, though the longer distance connection to LRV is maintained while connections to the POND or IWV vents is no longer found (Fig. 28). A channelized network would favor the expansion of flow paths that deliver water to vents with shorter straight-line distances, similar to the headward piracy of source areas by surface streams that exhibit larger gradients and thus greater stream power. Conversely the interconnected geometry of a distributed network would allow for the development of preferred pathways across steep hydraulic gradients, regardless of absolute distance.

Discharge Records:

A test of the isolated "northern" and "southern" drainage system interpretation can be made by comparing the discharge records from the two gauging stations (SGS and Little River). The majority of discharge from vents along the south western end of the ice terminus, including but not isolated to MEGA, MAM1, MAM2, POND and IWV vents, feed into the south fork of the Matanuska River (Fig. 4) and their discharge is recorded at the SGS gauging station. The discharge measured at SGS can be considered an average signal of the drainage system's response to surface melting and meteorological inputs. In contrast Little River gauging station measures only discharge water exiting LRV, indicating the response of a single drainage pathway to a single vent.

Assuming that the fluctuations of hydrologic inputs are similar over the study area as a result of local weather conditions, the details of the hydrograph should be related to the development of the internal drainage network (Theakstone and Knudsen, 1979). Any

differences in the discharge records between SGS and LRV is reasoned to be the result of the spatial heterogeneity of the overall drainage system and degree of interconnectedness between pathways feeding LRV and those of the larger network recorded at SGS.

Comparing the normalized discharge curves of these two gauges (Fig. 29) shows that during mid-meltseason (6/19/02-7/17/02, green and blue swaths on Fig. 29) when the average discharges recorded by SGS are increasing to maximum levels, there is little correlation between the records (r^2 = .0021, .0073 Pearson r = -.046, -.085) Although record exhibits the daily discharge fluctuations expected from insolation melting, time lags between the peaks and valleys are these trends in discharge extending beyond daily fluctuations do not coincide. Thus the LRV discharge record compared to that of SGS which averages discharge from of multiple vents suggests the northern drainage system is not linked to that of the south.

Both discharge records show a rapid increase at the onset of the melt season (yellow swath on Fig. 29), attributed by Ensminger and others (1999) to a rapid release of water stored subglacially because flow paths reduced or closed during the winter had not expanded enough to accommodate the increasing surface meltwater input. The rapid increase in discharge at all vents account for the high correlation between the records (r^2 = .915 or Pearson r = .957) at the beginning of the melt season (6/14/02 – 6/19/02). Peak flows however are generated earlier at LRV (6/26/02 and 7/1/02), while in the southern drainage network discharge increases to a mid-season maximum on 7/18/02 as recorded by SGS. I assume that subglacial inputs are increasing in the northern drainage basin from 7/1/02 to 7/18/02 as they are in the southern drainage, thus the falling discharge

recorded at LRV gaging station is explained by new unidentified exit points that connect to the subglacial pathways feeding LRV. The debris mantled ice near LRV may obscure any non-discreet releases of subglacial water, though this occurs between the vents of MEGA, MAM1, and MAM2 in clear ice, where silty subglacial water emits along numerous thin cracks and fissures during daily discharge highs (Fig. 30). From this evidence I suggest that the dominant pathways feeding LRV are unable to expand and accommodate the higher discharges and after the early-season peaks (6/26/02 and 7/1/02). The increased pressure force subglacial water to new exit points, enlargening the peripheral pathways that feed them and subsequently maintain a discharge when the pressures decrease, effectively "capturing" discharge that originally routed to LRV. The subglacial water exiting at these peripheral points would enter the groundwater system and be lost to the LRV gaging station.

The records are very well correlated during maximum system discharge at SGS (violet swath Fig 29, $r^2 = .896$, Pearsons r = .947) and remain in sync for the remainder of the field season, even during significant discharge swings (pink swath Fig. 25, $r^2 = .957$, Pearsons r = .978) (7/18/02-8/24/02).

The close correlation between the late season records of SGS and LRV is evidence that the individual LRV pathways have sufficiently expanded and connected with the overall drainage network and are now responding to meltwater input as a single combined drainage system. The charcoal results from run #12 in BH9 supports this interpretation (Table 1), with positive connections identified from BH9 to both LRV and MEGA vents indicating that subglacial water is flowing across a previous drainage divide

(Fig. 24).

Qualitative Analysis of Dye Return Curves

The comparison of individual dye return curves performed at different times is complicated by unknown daily variations in vent discharge (Nienow, 1996), as well as differences in the injection methods. Yet the data shows a broad spatial heterogeneity during the course of the melt season.

A qualitative look at two very dissimilar dye return curves (Fig. 31) can be used to elucidate the differences in dye return curves, and hence in flow paths, that can occur at locations near the glacial terminus. The rapid and tightly peaked curve of MAM1 contrasted with the breadth, multiple peaks, and asymmetry of the rising and falling limbs of the curve captured at POND. The differences highlight a flow path from BH6 to MAM1 that moves water rapidly through efficient channels producing a single return peak. In contrast, a system of inefficient pathways from BH5 to POND of varying lengths and possible storage retardation produces the aggregate of multiple independent dye clouds following varying flow paths (Seaberg et al. 1988; Hooke, et. al., 1988; Willis et al. 1990).

Quantifying Conditions of Flow

Quantified differences between individual dye curves provide more details on the specific flow paths, when considered within the larger framework of a distributed

drainage network beneath the Matanuska Glacier's terminus.

The quantitative analysis of breakthrough curves requires the calculation of parameters that characterize the conditions of flow during transit of the dye cloud; average linear velocity (u, ms^{-1}), dispersion coefficient (D, m^2s^{-1}), and dispersivity (d, m). These parameters were calculated from the smoothed breakthrough curves (Figs. 5-19) by applying the equations derived by Brugman (1986) and subsequently described by Nienow et al., (1996) as

$$u = x / t_m \tag{1}$$

$$D = \frac{x^2 (t_m - t_i)^2}{4 t_m 2 t_i \ln\left(2(t_m / t_i)^{1/2}\right)} \tag{2}$$

$$d = D / u \tag{3}$$

where x is the straight line distance from injection site to the collection vent, t_m is the time to peak concentration (treated as a variable to be solved by the equation, not taken from the curve), and t_i as the time when half of the peak concentration was recorded.

The dispersion coefficient (D) is described as the rate of dye cloud expansion from the point of injection (Hasnain, 2001). In a perfect still body dispersion would result from chemical diffusion of the dye from the initial point of injection to surrounding areas of lower concentration. In a flowing channel, dispersion results primarily from the variation of velocity within the channel (Seaberg et al., 1988) and can be envisioned as the expansion of a plume of smoke from an extinguished candle due to the turbulent flow of the rising hot air. Within the subglacial system dispersion can result from the velocity difference of a smaller tributary channel entering a larger trunk channel or as the

combined velocity differences of dye traveling along multiple distributed flow paths. Thus, a degree of dispersion is expected in both a channelized and distributed subglacial network.

Equation 2 represents two separate equations that are defined for $i = 1$, the time when half the peak concentration is recorded on the rising limb, and $i = 2$ when the concentration is recorded on the falling limb. The two equations are solved iteratively by choosing a value for t_m that satisfies the two equations with respect to a common D value (Nienow et al., 1996). Since a high dispersion rate can result from either the tortuosity of high velocities in channelized flow or from multiple length scale flow paths in a distributed network, dispersivity *(d)* has been employed as an index to the complexity of a drainage pathway (Seaberg et al., 1988, Hooke and Pohjola, 1994). Defined as the relationship of the rate of dispersion relative to the velocity of the dye cloud as it travels through the drainage pathway, dispersivity can be interpreted as an index scale of the actual length of the exiting dye cloud (Seaberg et al., 1988, Hooke and Pohjola, 1994). Figure 32, shows conceptually how two dye clouds traveling equal distances (x_1 to x_2) with different dispersivity values would be represented by the recorded dye breakthrough curve.

The dye concentration values that resulted from the connection between BH8 and MAM2 during run #11 (Fig. 16) and the connection between BH9 and MEGA of run #12 (Fig. 18) show two distinct curves within each record. With the assumption that each curve represents an independent flow path, metrics were calculated individually and denoted as "(A)" and "(B)" within Table 2. It is important to note that these metrics do

not make any reference to overall system complexity since the curves are treated independently.

Breakthrough Curves Metrics

Table 2 summarizes the data calculated from the fifteen breakthrough curves collected during the dye injection tests.

Dye Recovery

Multiple factors influence what quantity of dye will be recovered during an individual injection experiment. These factors are: 1.) the successfulness of sampling at every known and unknown exit point for subglacial water that contains measurable quantities of dye. 2.) The successfulness of sampling over a duration that captures the total length of the exiting dye cloud. 3.) The quantity of dye lost from the affects of adsorption onto mineral surfaces within transit (Kasnavia et al., 1999). 4.) The quantity of dye lost from storage within the subglacial system and flow into the groundwater system. The data required to resolve the latter two factors are beyond the scope of this project and further investigations would need to be conducted in order to gauge their significance at this study site.

The recovery rates calculated at LRV (the only vent where discharge could be measured and thus recovery calculations performed) show that only once, early in the melt season, did the majority of the dye mass exit through a sampled vent (Run #5, Table 2). Subsequent experiments from the same injection site (BH5 run #7 and #14) yielded progressively lower recovery percentages during the course of the melt season. These

results highlight the caveat that the individual dye curves may not characterize the flow paths of the majority of the subglacial system; instead, they may highlight only those flow paths where water exits at a discreet vent location. The low recovery rates at LRV and lack of any additional connections as shown by the charcoal bugs suggests that the drainage network may discharge a significant percentage of subglacial water at points unidentified by the author.

Velocity, Dispersion, and Dispersivity:

Average linear velocity calculations do not take into consideration the degree of sinuosity along a flow path and therefore are considered minimum values for the actual flow velocity (Seaberg et al., 1988). Because of this velocity calculations should not be used to determine the flow path's geometry but instead speak to the degree of complexity of the drainage system as compared to previous studies and the observed differences between repeated borehole to vent connections.

Assuming that the high velocities (avg. 0.33m/s Figs. 11,12,13 and Table 2) recorded from injections at BH6 represent a channelized flow path, the lower velocities calculated from the remainder of tests (avg. 0.053m/s) agree with values reported by previous studies of flow across glacier bed overdeepenings where distributed flow is expected (Lawson et al.,1998; Hooke and Pohjola, 1994; Seaberg et al.,1988; Hasnain et al., 2001). . Similar length scale experiments on the Matanuska Glacier by Lawson et al. (1998) yielded a velocity of 0.04 m/s. These values from the Matanuska Glacier are also consistent with those reported by Hooke and Pohjola (1994) of 0.011 - 0.089 m/s from an

overdeepening of Storglaciären, Sweden. Typical velocities of 0.024 to 0.042 m/s reported by Brugman (1986) from the Variegated Glacier, AK are attributed to a widely distributed drainage system developed during a period of surging advance, while post-surge flow velocities averaging a faster 0.7 m/s were attributed to a channelized system.

The order of magnitude higher velocities (avg. 0.33m/s) calculated from connections made between BH6 and both MEGA and MAM1 vents (Runs #8,10, Table 2) are consistent with the velocities of channelized systems such as the post surge velocities reported by Brugman (1986), those of Seaberg et al. (1988) (0.30 to 0.69 m/s), and those of Hasnain et al. (2001) (0.37 to 0.47 m/s). My velocity data supports suggests a widespread distributed drainage network upglacier with low flow velocities, but include localized, high velocity, channels near the terminus where there has been apparent enlargement of drainage conduits.

To understand differences between linear velocity calculations from experiments under similar discharge conditions two conditions must be considered. First, the actual flow velocities are similar but the total length of the flow path (sinuosity) is greater due to increased drainage complexity. Or the flow velocities vary in response to changes in the hydraulic geometry of the system along similar, static length flow paths (Nienow et al., 1996). Because discharge data is lacking for the majority of individual vents there is the interpretation of velocity differences amongst individual tests cannot be made except for the LRV vent where discharge values are available.

An unpressurized subglacial channel follows the general stream power law relationship: increases in velocity correspond to increases in discharge (Nienow et al.,

1996; Kohler, 1995; Seaberg et al. 1985). Nienow et al., (1996) show that the expected relationship can reverse as discharges exceed the capacity of channels to transport higher volumes thus producing pressurized flow paths. Within a distributed network decreases in discharge, with a corresponding drop in water pressures, allow a greater percentage of the subglacial water to route through the most efficient flow paths, thus producing a drop in the average linear velocity of an exiting dye cloud . The velocity results of the BH5 to LRV connection suggest that this near terminus system is influenced little by decreasing discharges (solid lines, Fig. 33a & b). I conclude from the evidence that a consistent condition of high basal water pressure exists near the terminus throughout the melt season, creating a hydraulic bottleneck that maintains the low recorded velocities. This interpretation is supported by field observations of relatively consistent fountain heights at the vent and consistent water level heights in near terminus boreholes that are independent of changes in the daily discharge volumes (Larsen, 2001).

In contrast, the farther up ice connection of BH2 to LRV exhibits an increase in velocity corresponding to lower discharges later in the melt season, suggesting a reduction in the number and/or lengths of individual flow paths as the lower water volumes moved faster through the evolved subglacial system (dashed line Fig. 33b). The decreasing value of dispersion and dispersivity (dashed lines, Fig. 33c & d) support the conclusion that the dye cloud traveled more efficiently from the father injection point later in the season, producing a tighter spread in dye concentration values as compared to the earlier test when a higher sinuosity is suspected.

If we combine the results from the near terminus BH5 injections and the farther

up ice BH2 injections, we may assume that water traveling through the subglacial system in the northern part of the study experiences a change in its flow conditions as it approaches the terminus. At distances greater than 250m from the terminus, subglacial water travels through a network that becomes backed up during times of high seasonal discharge, though as discharge drops, water travels faster though fewer, larger channels. At some distance less than 250m from the terminus, water enters a network that is characterized by near constant hydraulic restrictions, maintaining high water pressures and slow velocities until exiting the subglacial system.

The next analysis will focus on the experiments within the southern section of the study area. Successful injections were conducted within a short time span during a period of steady seasonal discharge (Fig. 20 run# 10-12). Because of this relationship, I will consider the differences between these experiments as predominately a result of injection point location, rather than flow volume. In order to interpret the test results as a function of increasing injection distance from the terminus, the metrics recorded by the MEGA and MAM1 breakthrough curves during each experiment are considered as one. I base the validity of this analysis on from the similarities of the vents' dye breakthrough curves and the vents' close proximity to one another. Results from a single curve collected at MAM2 vent were not considered since there was no basis for comparison.

From Figure 34a, we see that as the distance from injection point to the terminus increases, average linear velocities drop, suggesting that the drainage pathways enlarge in the down ice direction. The low dispersivity value calculated from the near terminus injection point (Table 2, run #10) and the shape of the breakthrough curve (Fig. 13)

confirm that the dye cloud is traveling as a single pulse, most likely restricted in a limited number of large, unobstructed channels. To explain the highest calculated values of dispersion and dispersivity from the ~500m injection distance (BH8) (Fig. 34b,c), we must envision the dye cloud separating early after injection and following two dominant flow paths, until rejoining near or at the terminal vents. The resultant curves at the exit vents (Fig. 14, 15) would be considered a summation of two or more tightly constrained breakthrough curves following disparate flow paths. The support for this conjecture is shown at the farther ~800m injection distance where two distinct peaks within the breakthrough curve are indeed found (Fig. 18, run #12). The increased travel distance at the farther injection point allows for the further separation of the dye clouds and subsequently two peaks within the breakthrough curve (delineated as (A) & (B), Table 2, run #12) with lower individual dispersion and dispersivity values (Fig 30b,c).

To summarize, calculated metrics of the MEGA and MAM1 vent breakthrough curves show multiple low velocity flow paths that converge at some distance (~500m - 300m) from the terminus and enlarge to unrestricted channels feeding the discharge vents. The interpretation is similar to the composite flow paths reported by Hasnain et al. (2001) and Nienow et al. (1998) that show the headward growth of hydraulically efficient trunk channels into an up-ice distributed network over the course of a melt season.

Regardless of interpretation, the results from these "southern" injection experiments show that the subglaical flow conditions are unlike that of the northern part of the study area and are determined by some factor(s) other than meterologic conditions.

Conclusions:

The field observations and dye tracer studies conducted at the Matanuska Glacier in 2002 support the following interpretations of the characteristics of the subglacial drainage system within the study area:

- Charcoal bug sampling shows that single point injections of a tracer often result in multiple connections to discharging subglacial vents in the down ice direction (Fig. 21-24). Increases in the number of borehole to vent connections from repeated tests during the melt season suggest an expansion of local drainage networks as the system matures to accommodate higher discharges. (Fig. 23,24)
- Charcoal bug sampling shows that individual injection points connect to spatially segregated terminal vents, defined as "northern" and "southern" vents, during the early melt season (Fig. 21-23). Segregation of the drainage within the study area ends later in the melt season due perhaps to expansion and connection of the local drainage networks (Fig. 24)
- Semi-qualitative dye concentrations eluted from charcoal bug samples supports a distributed network for the northern part of the study area. (Fig. 25,27,28)
- Discharge records show that the local drainage network delivering water to Little River Vent does not correlate to the overall system's response to the

same meterological inputs early in the melt season. A late season correlation between the records suggests expansion and connection of the Little River drainage network to the greater system network (Fig. 29).

- Gaging station records and field evidence show that the discharge at Little River Vent peaks and then declines during a period of increasing discharge for the overall subglacial system, suggesting that hydraulic bottlenecks within the local system force water to peripheral exit points which expand and capture discharge that previously exited at LRV (Fig. 29, 30)
- Quantitative metrics from dye breakthrough curves at Little River Vent show that the northern drainage system is characterized by multiple pathways that restrict flow in a near terminus distributed system regardless of changes in discharge volumes. (Fig. 33)
- Quantitative metrics from dye breakthrough curves at MEGA and MAM1 vents show that the southern drainage system is characterized by multiple pathways that coalesce and expand in size as they approach the terminal vents. (Fig. 34)

Future study would focus on the delineation of the observed spatial differences in network complexity in comparison with the underlying bed morphology. If the presence of localized distributed drainage at the Matanuska Glacier can be shown to be the result of bed morphology and the physics of frazil ice growth as reported by Alley et al. (1998), then these important factors can be utilized in future models of sediment transport and glacier velocity (Hubbard et al., 1995; Ensminger et al. 1999).

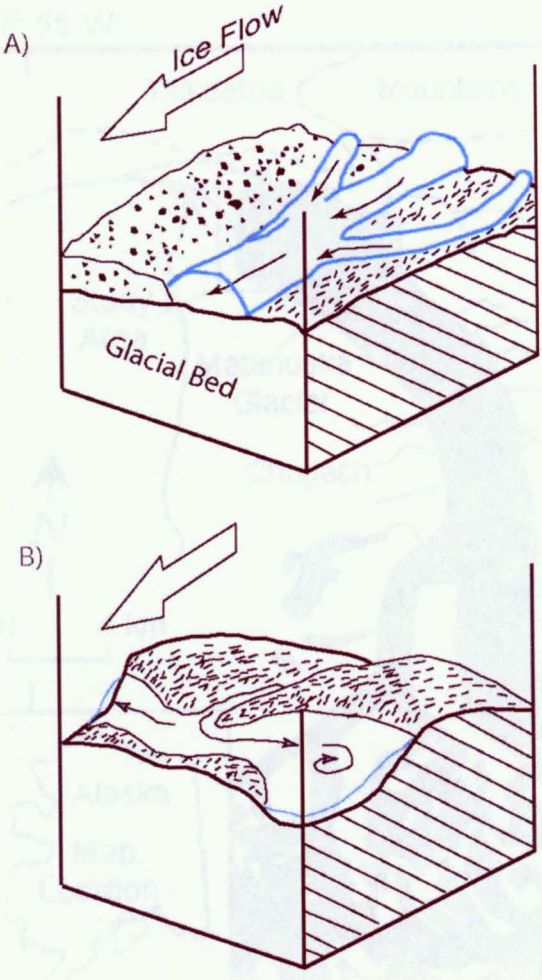

Fig. 1A) Idealized drawing of a discrete subglacial drainage system, composed of arborescent conduits. B) Idealized drawing of a distributed subglacial drainage system composed of a series of narrowly linked cavities (modified from Hubbard et al., 1995).

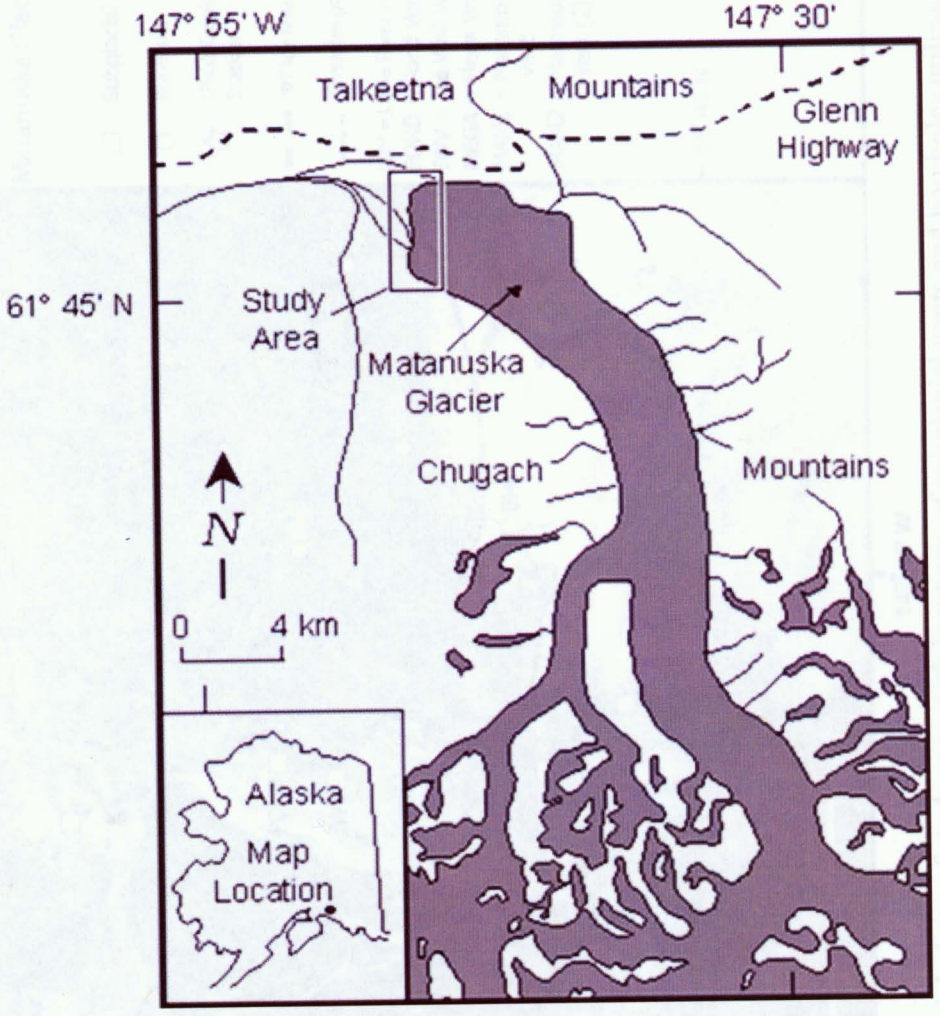

Fig.2 Study area at the Matanuska Glacier, AK (modified from Lawson et al., 1998).

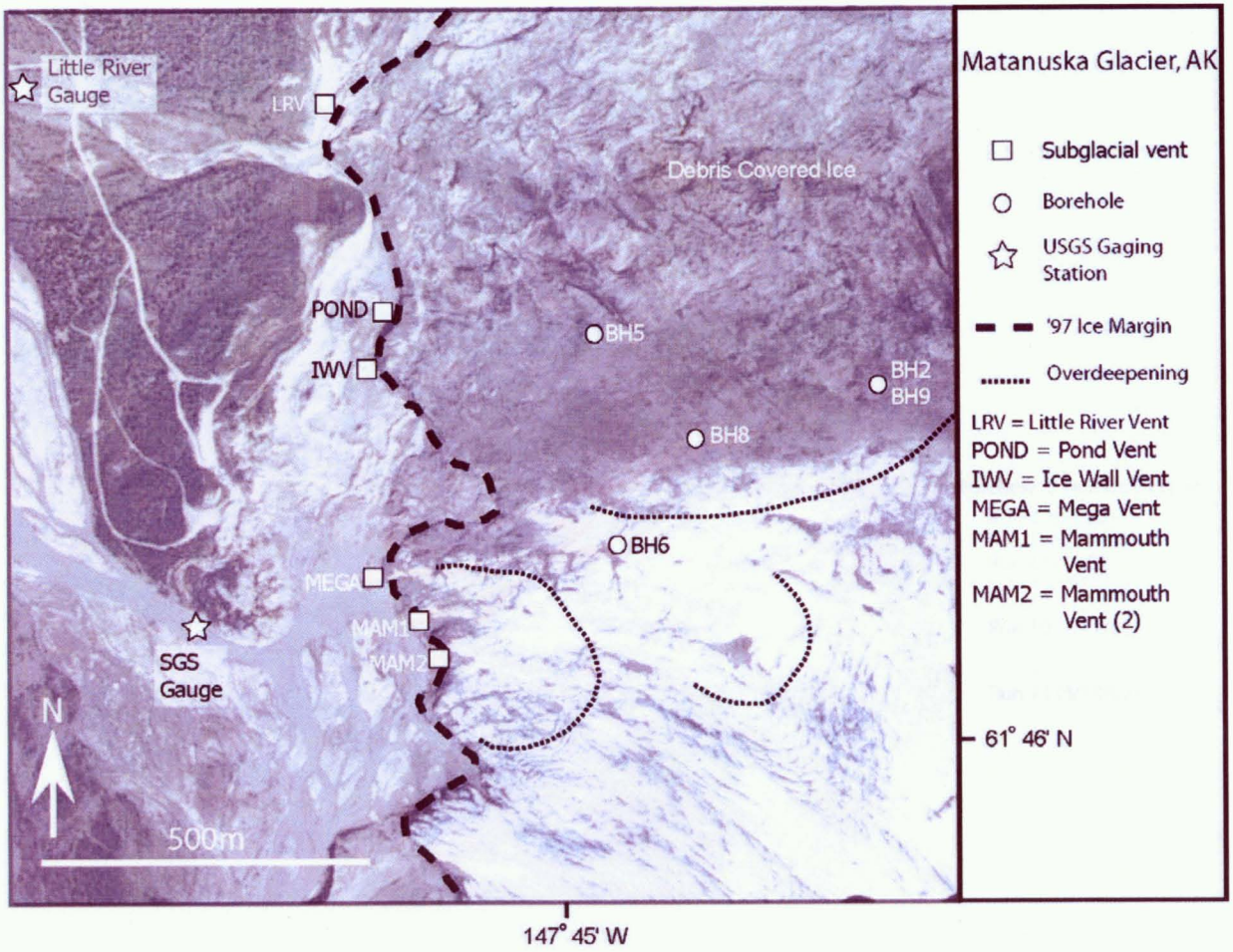

Fig.3 Arial photo of study area with locations of subglacial vents and boreholes utilized during the investigation.

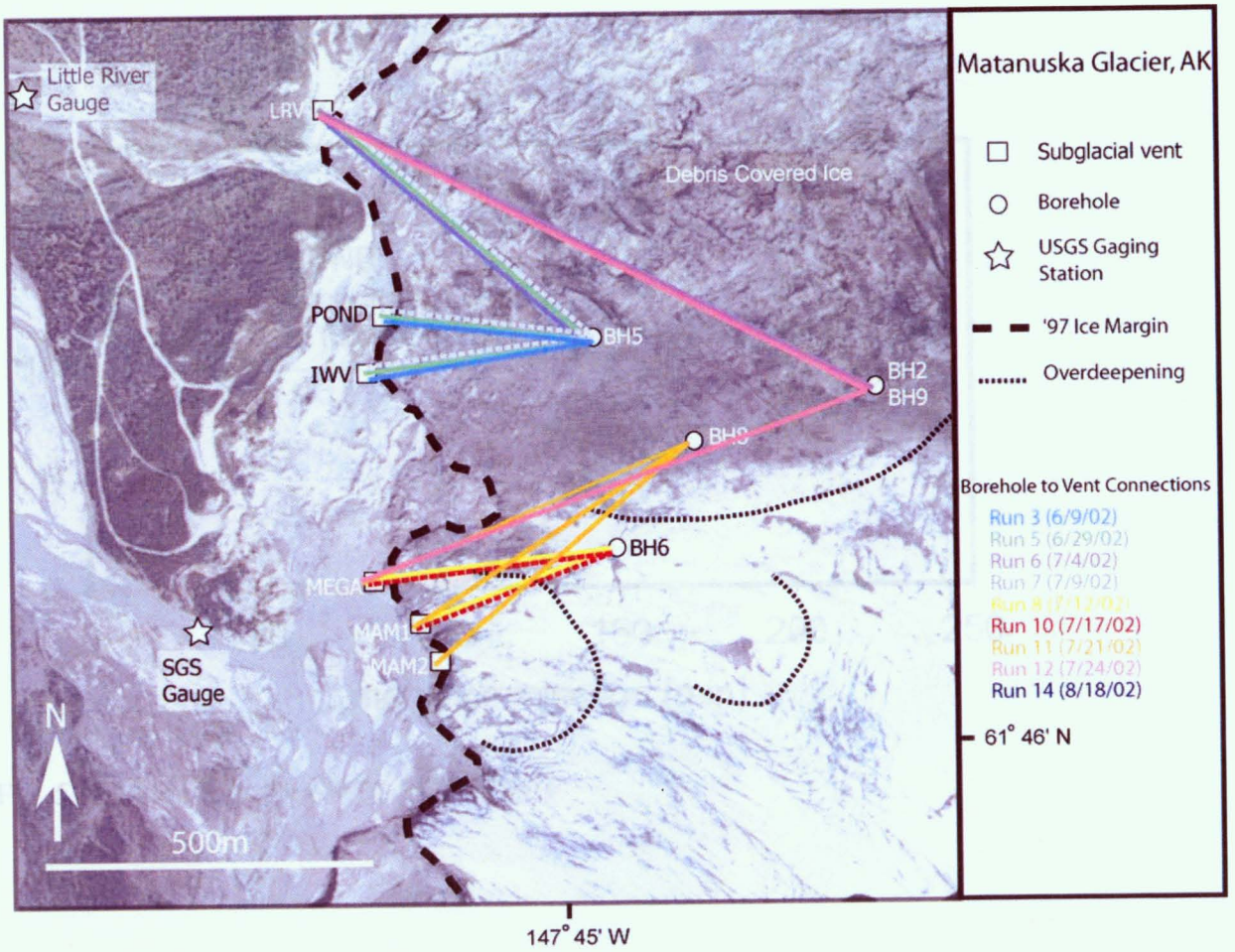

Fig. 4 "Strong" and "weak" borehole to vent connections (colored lines) made during each dye injection experiment.

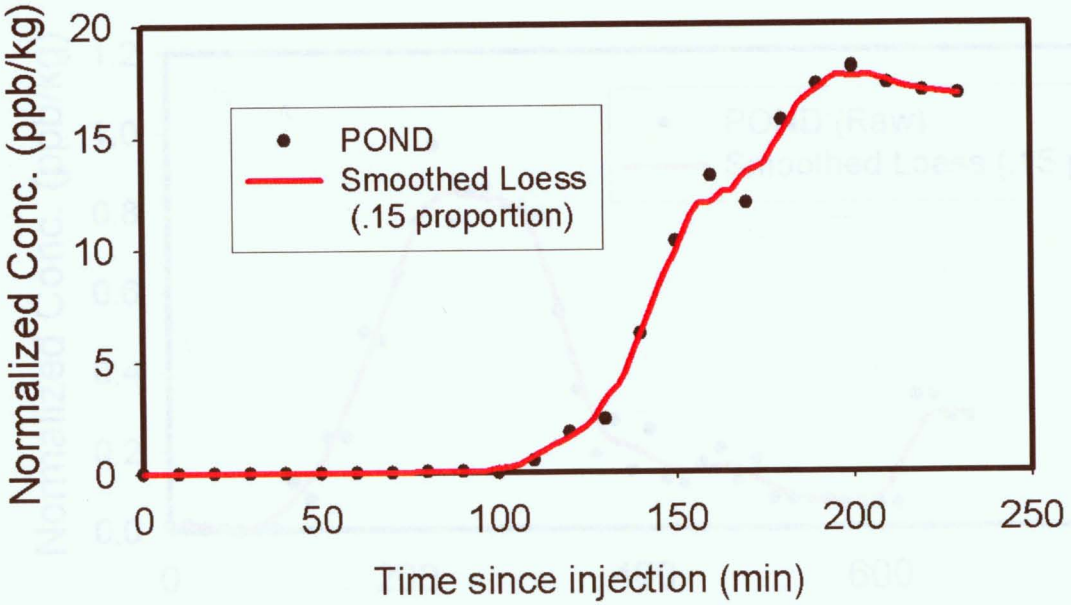

Fig. 5 Injection Run #3: 6/9/02 BH5-POND

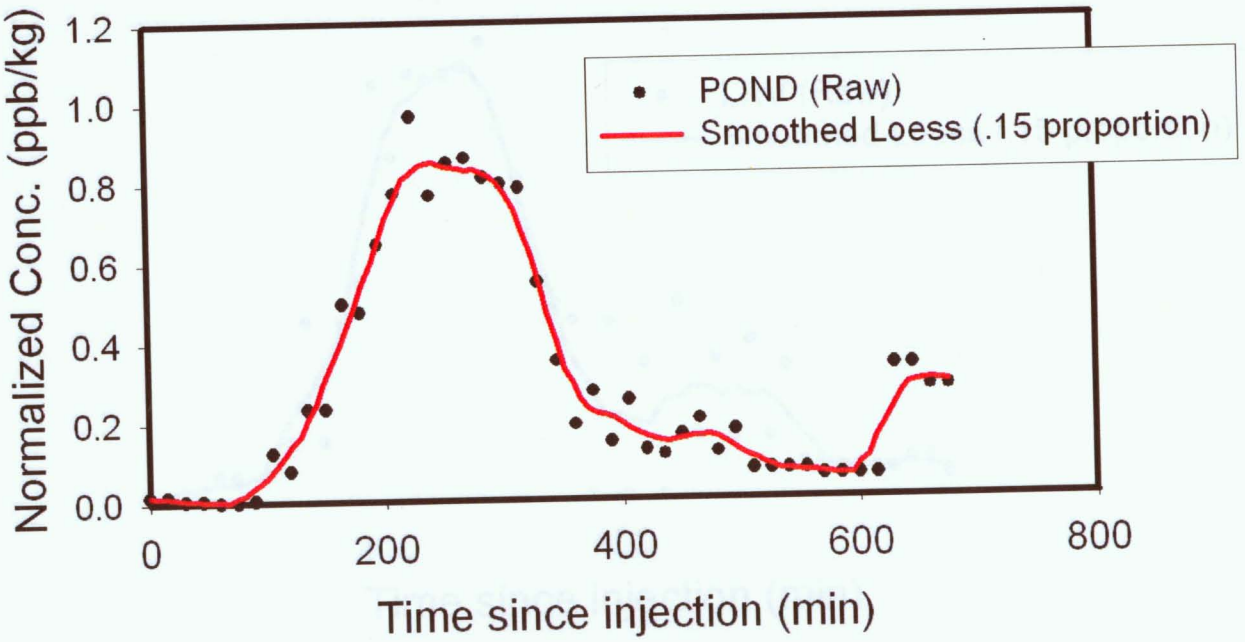

Fig. 6 Injection Run #5: 6/29/02 BH5-POND

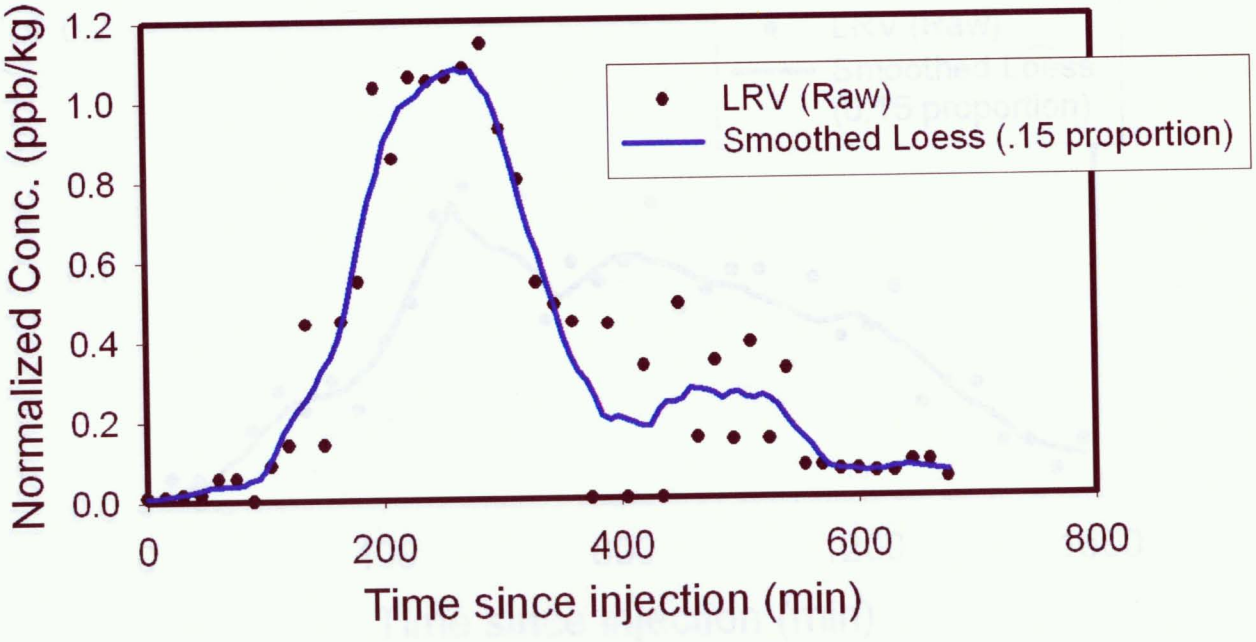

Fig. 7 Injection Run #5: 6/29/02 BH5-LRV

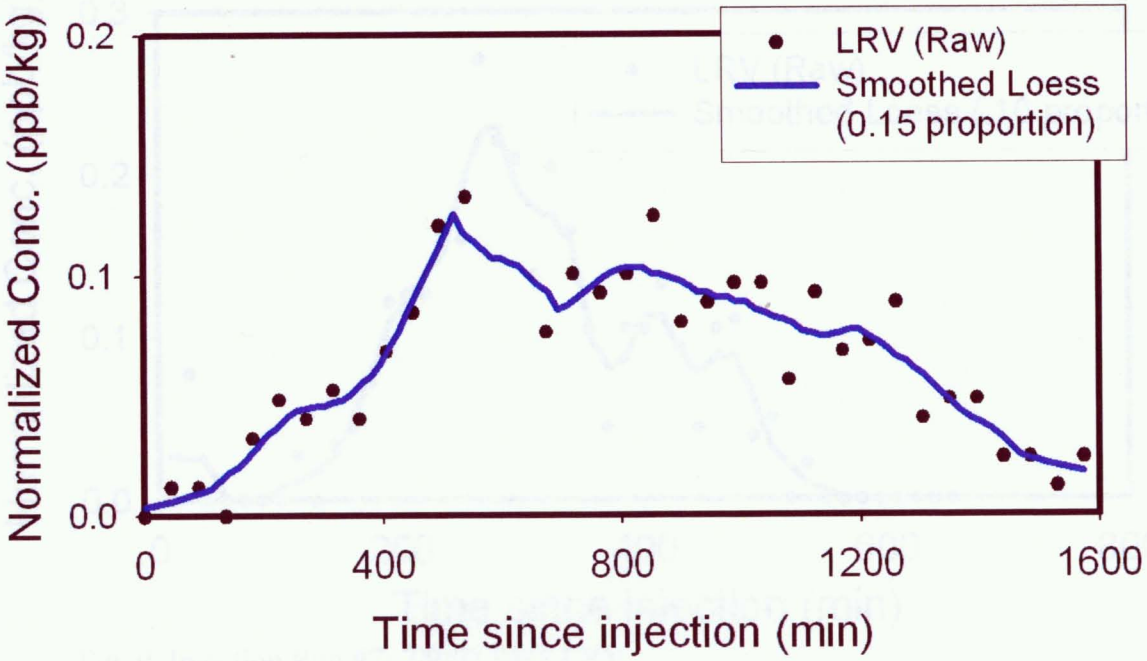

Fig. 8 Injection Run #6: 7/4/02 BH2-LRV

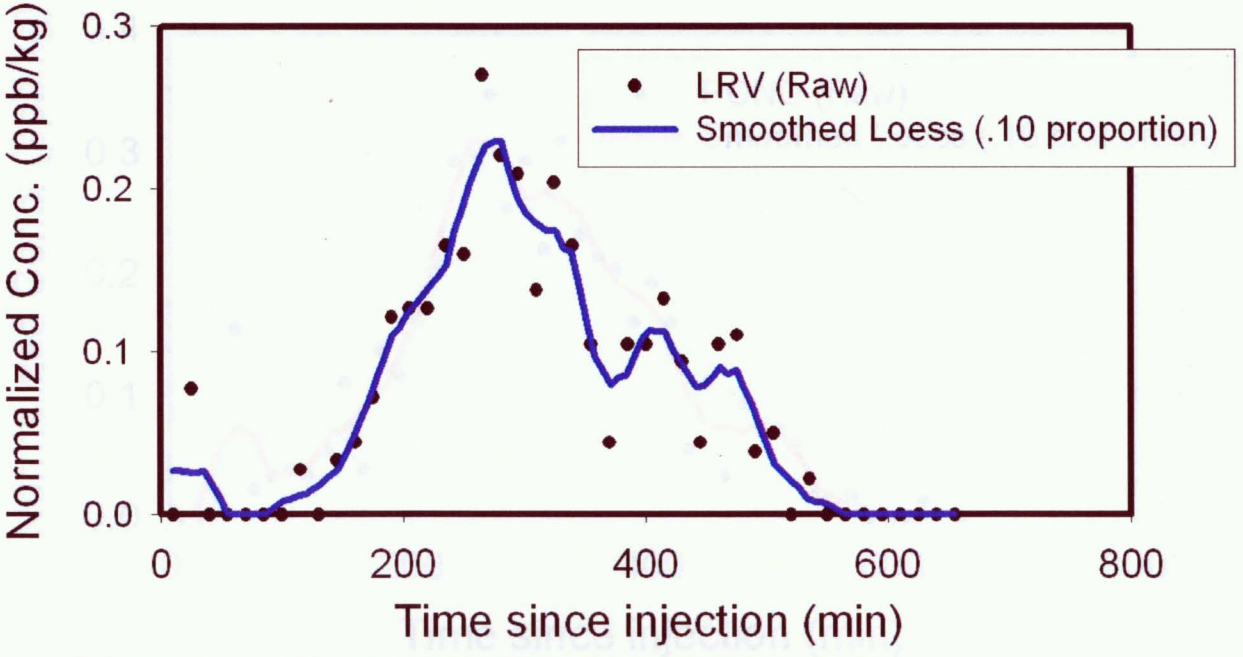

Fig. 9 Injection Run #7: 7/9/02 BH5-LRV

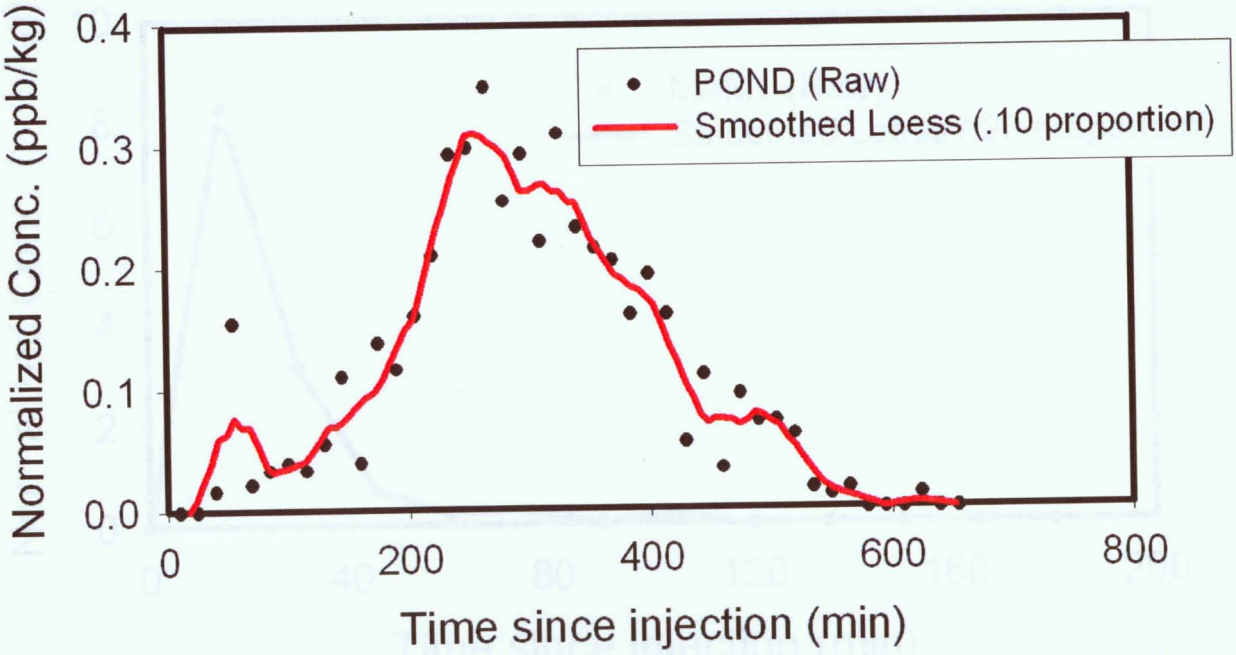

Fig. 10 Injection Run #7: 7/9/02 BH5-POND

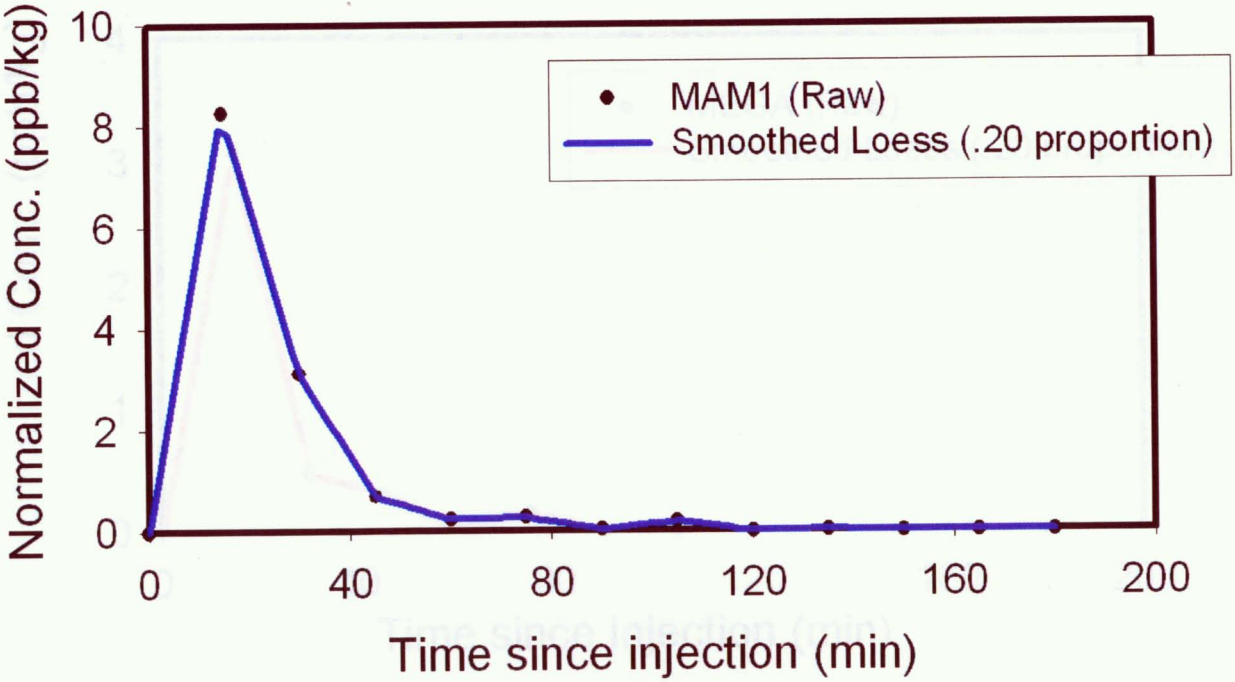

Fig. 11 Injection Run #8: 7/12/02 BH6-MAM1

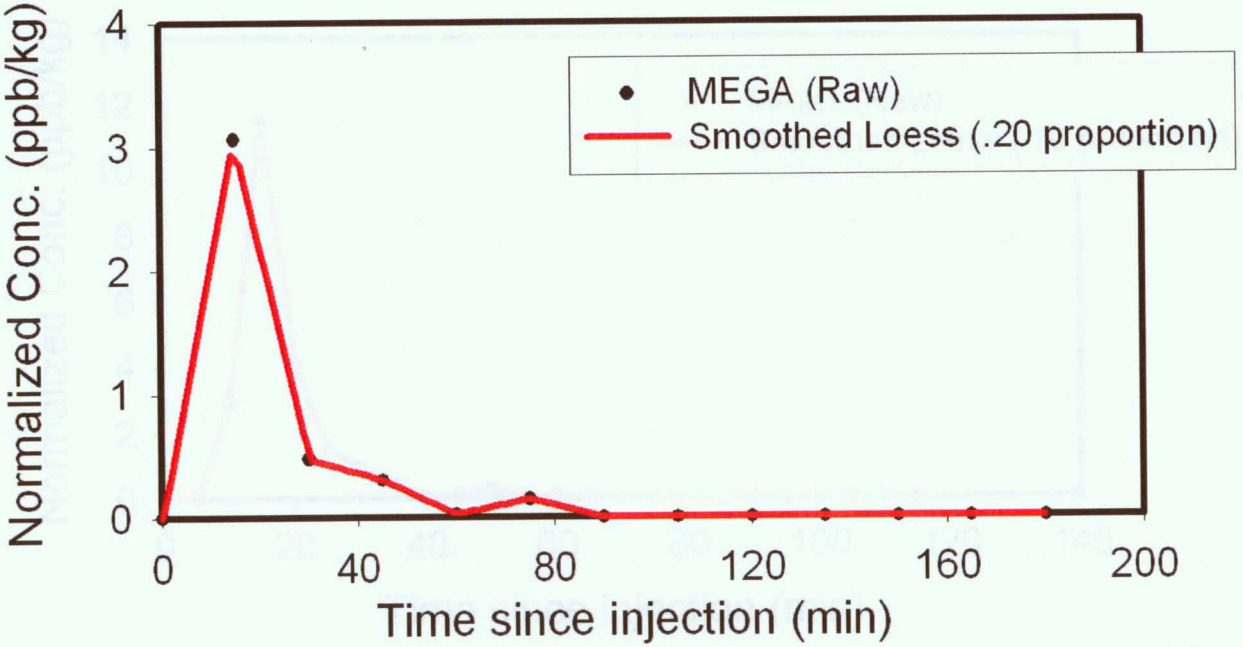

Fig. 12 Injection Run #8: 7/12/02 BH6-MEGA

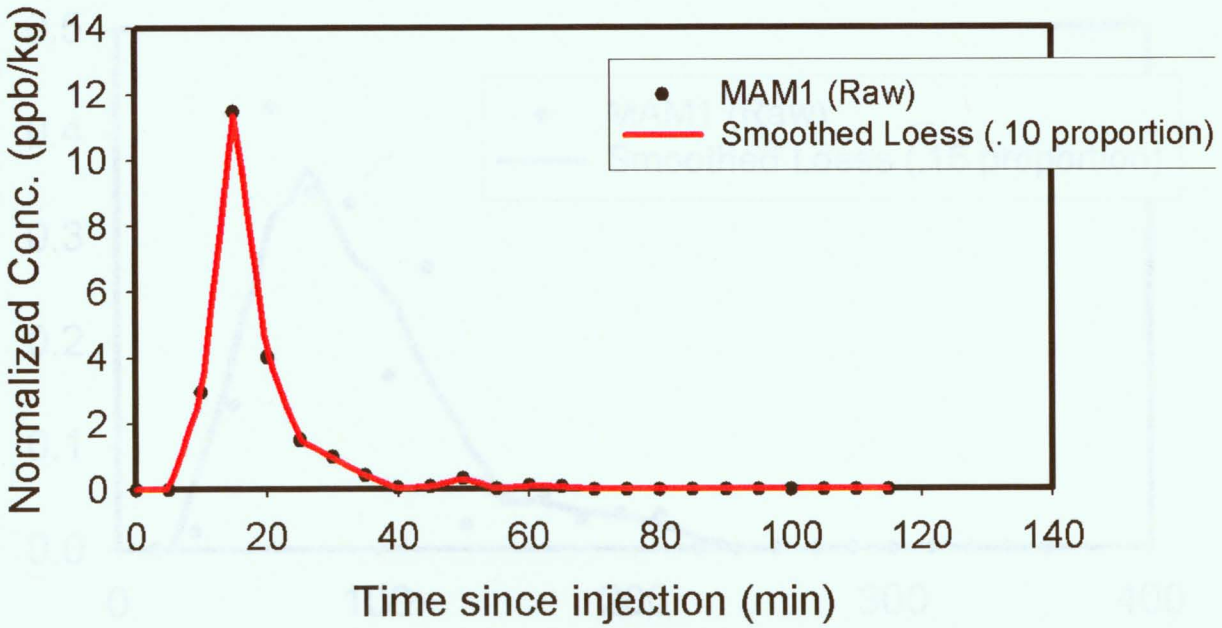

Fig. 13 Injection Run #10: 7/17/02 BH6-MAM1

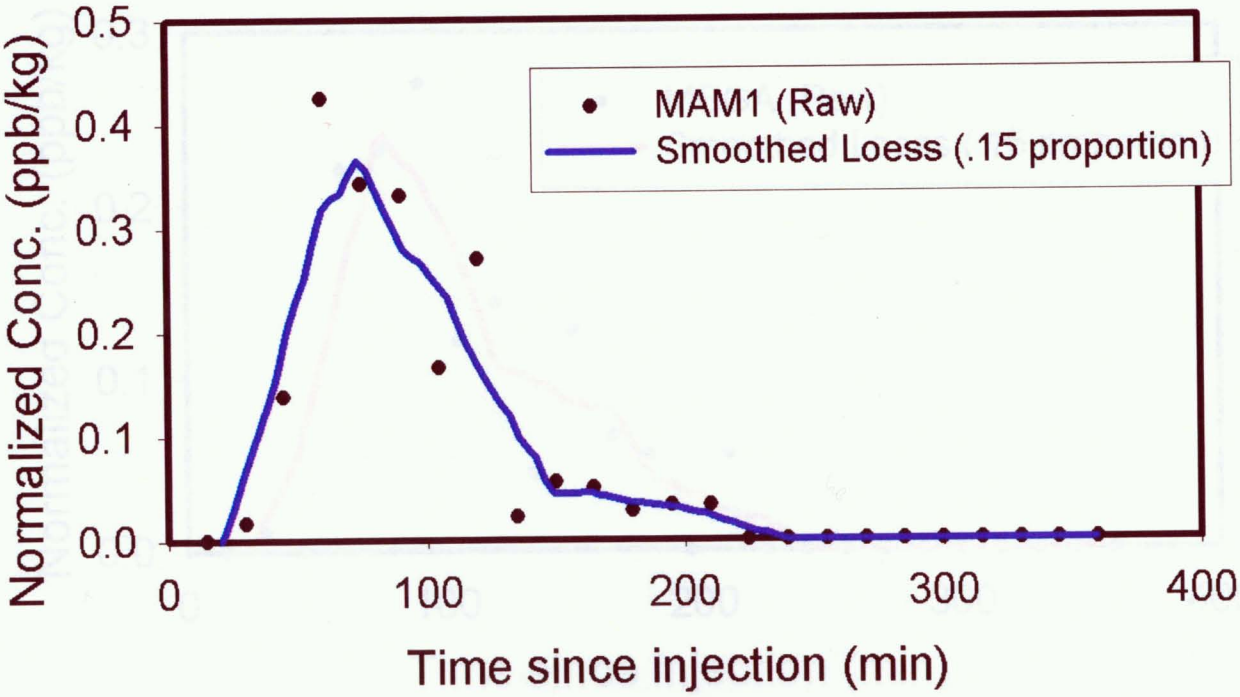

Fig. 14 Injection Run #11: 7/21/02 BH8-MAM1

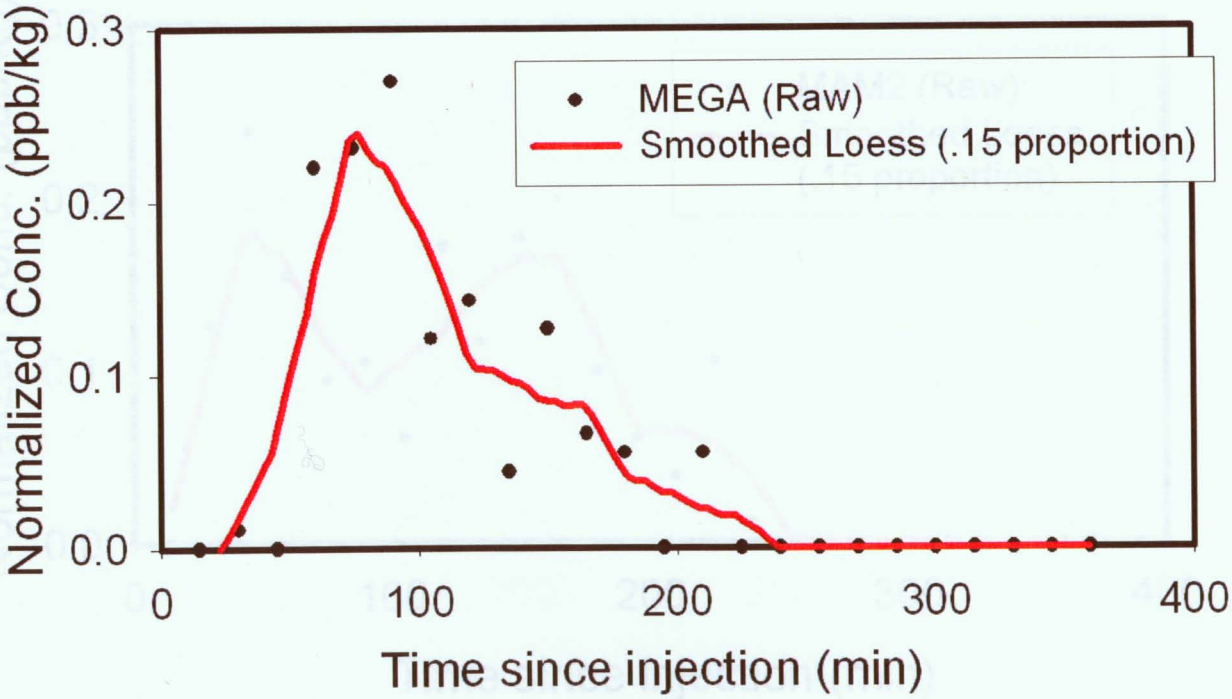

Fig. 15 Injection Run #11: 7/21/02 BH8-MEGA

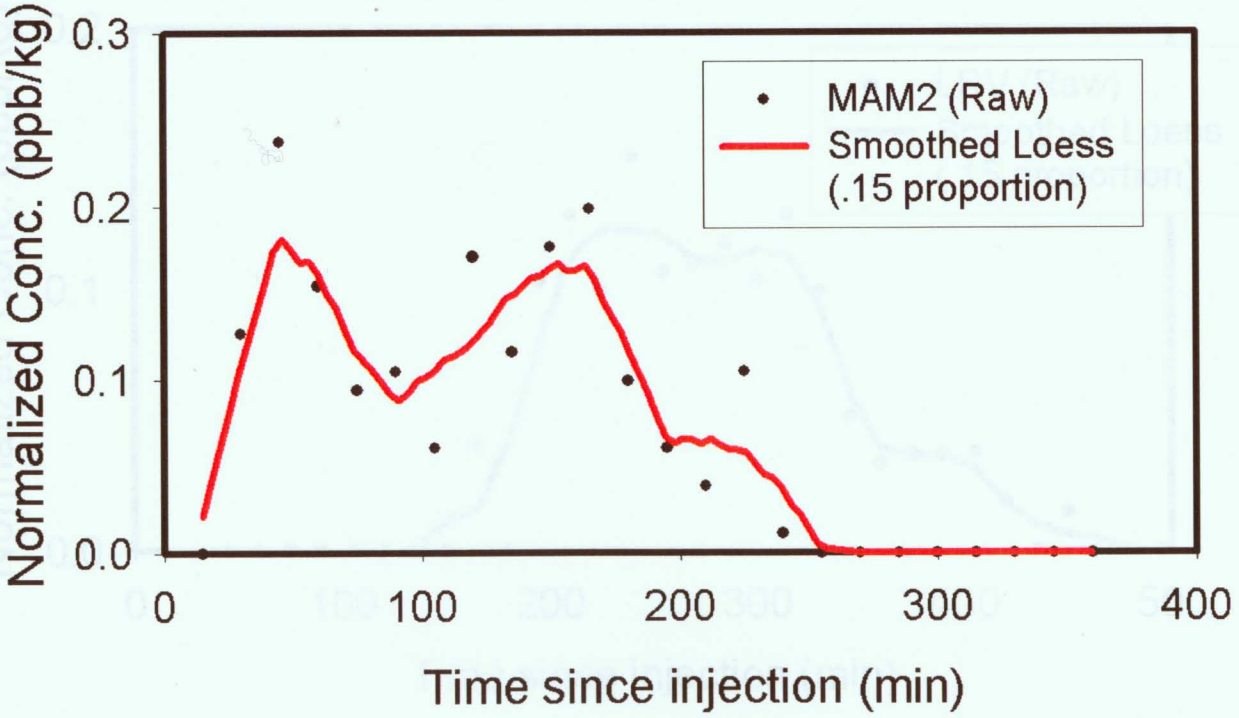

Fig. 16 Injection Run #11: 7/21/02 BH8-MAM2

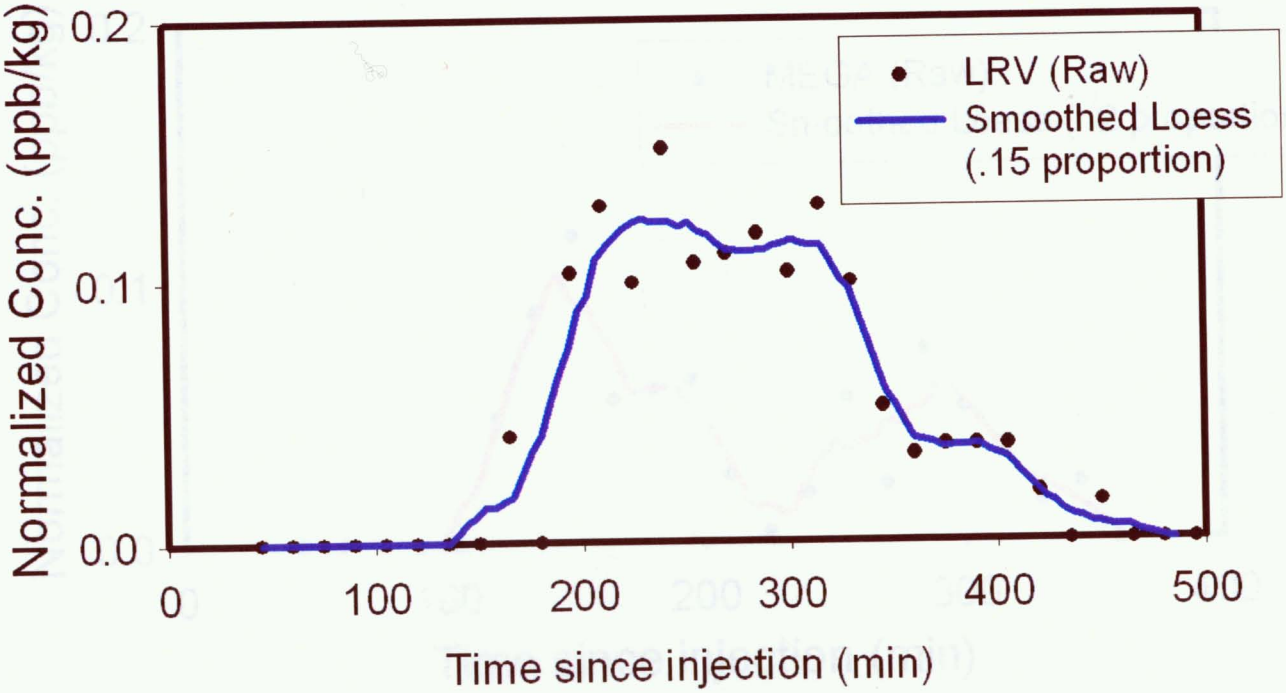

Fig. 17 Injection Run #12: 7/24/02 BH9-LRV

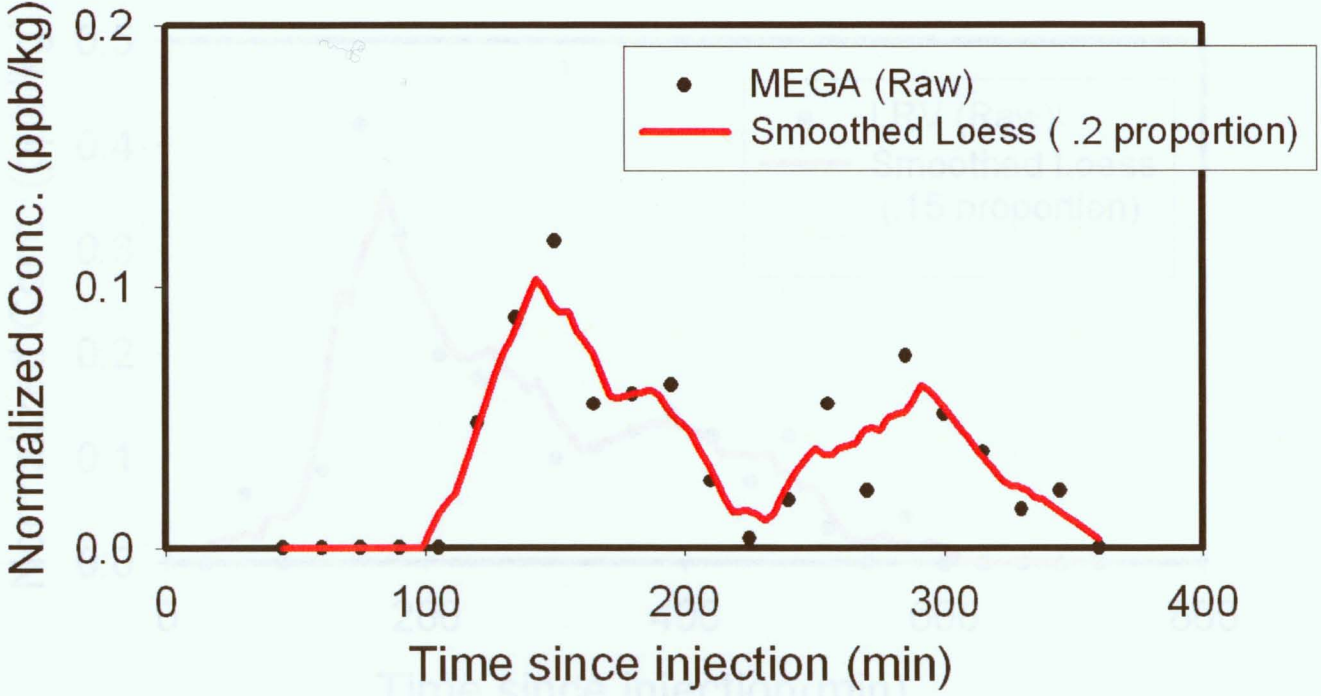

Fig. 18 Injection Run #12: 7/24/02 BH9-MEGA

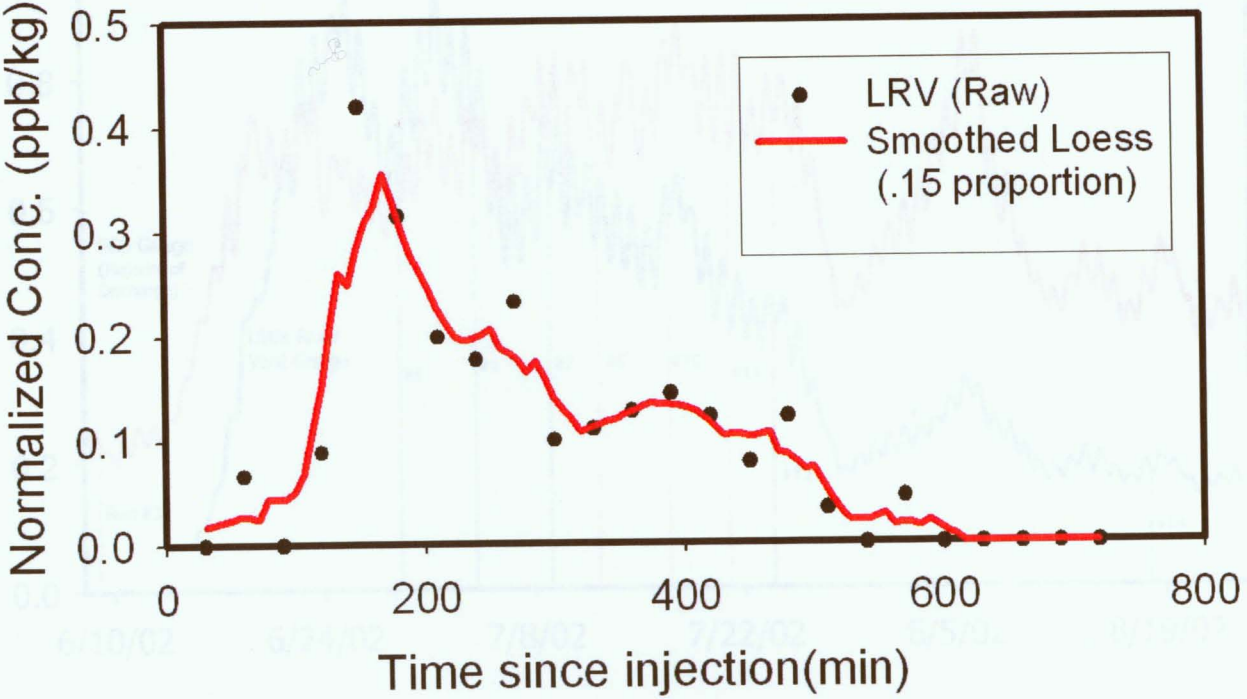

Fig. 19 Injection Run #14: 8/18/02 BH9-MEGA

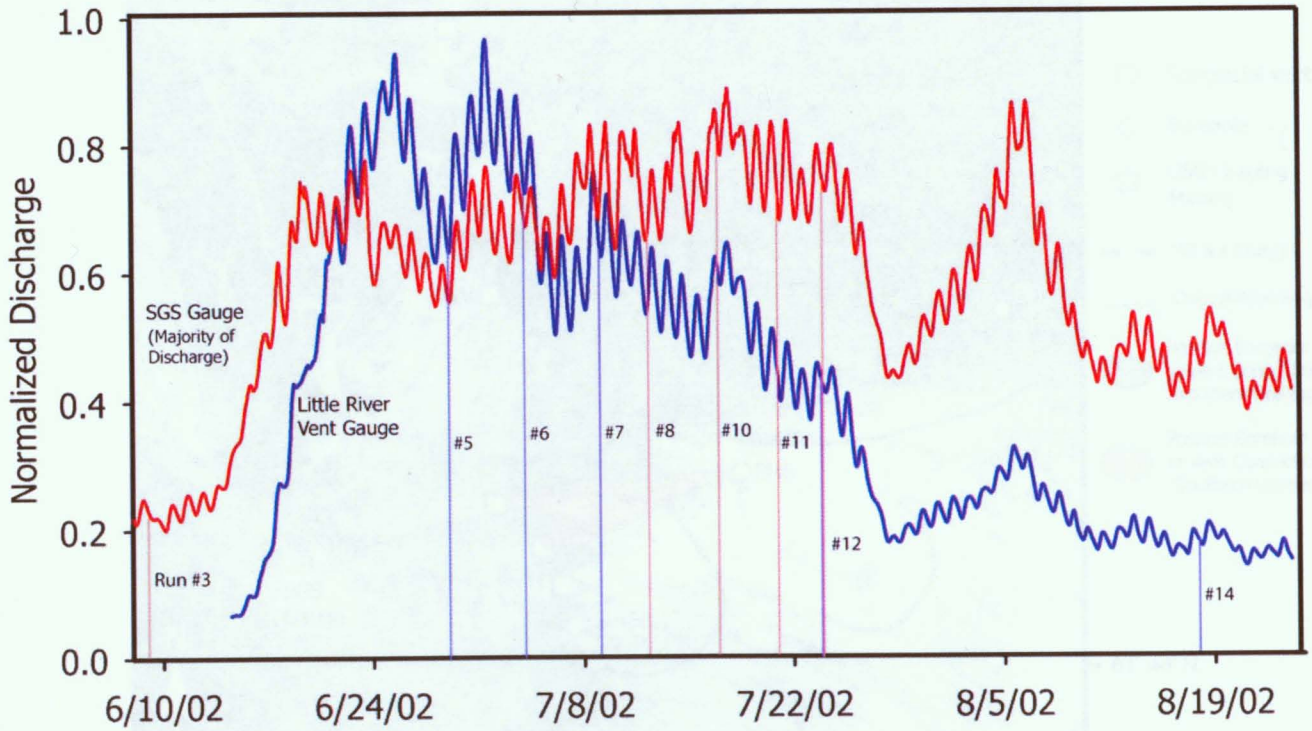

Fig. 20 Normalized discharge records from Little River Gauge (blue) and SGS Gauge (red) recording the combined discharge of glacial vents creating the south fork of the Matanuska River. Vertical lines indicate the timing of individual dye runs in which return curves were collected and the corresponding discharge record used for interpretation.

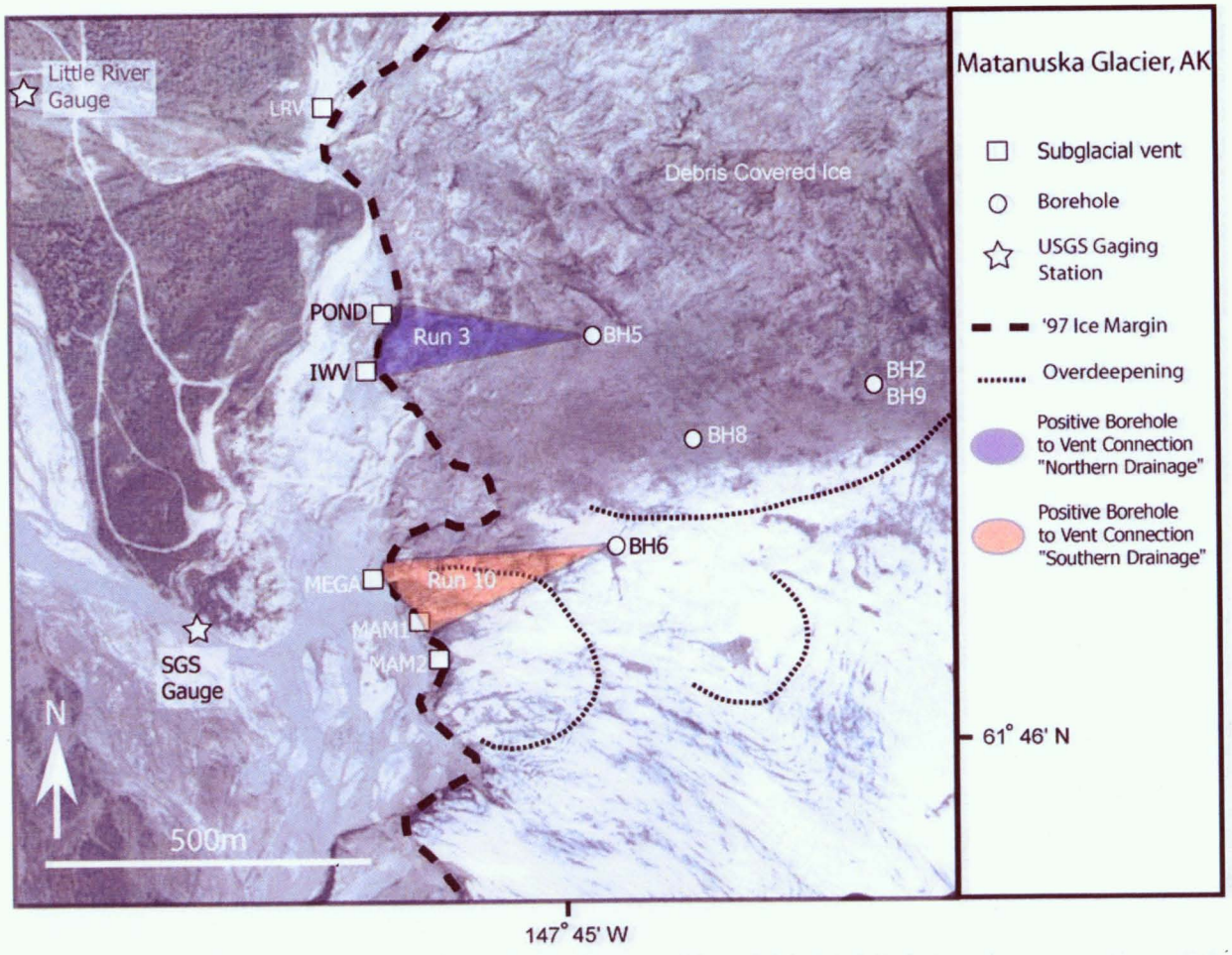

Fig. 21 Borehole to vent connections from near terminus runs #3 and 10.

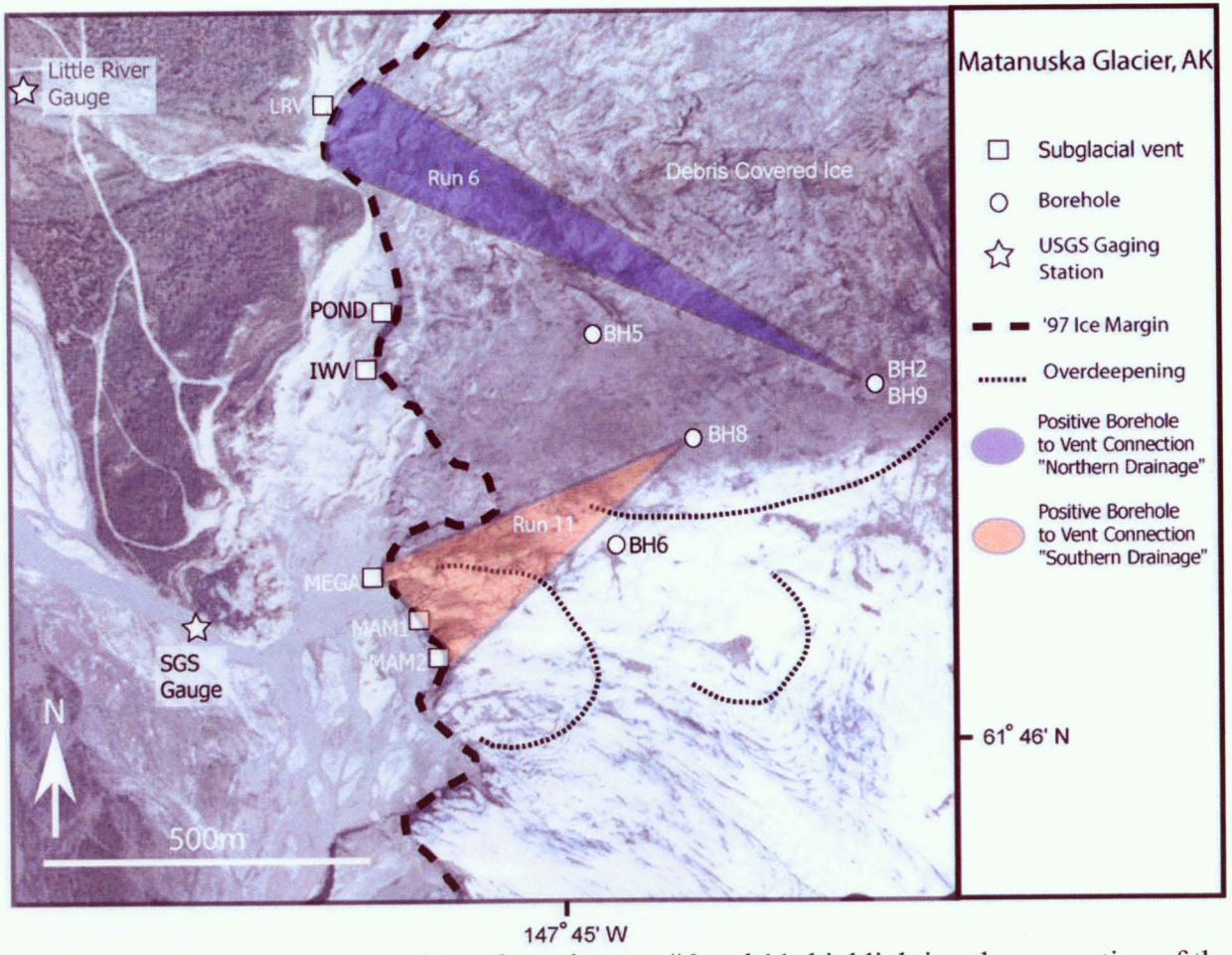

Fig. 22 Borehole to vent connections from dye run #6 and 11, highlighting the separation of the northern and southern drainage networks at the furthest injection points from the terminus.

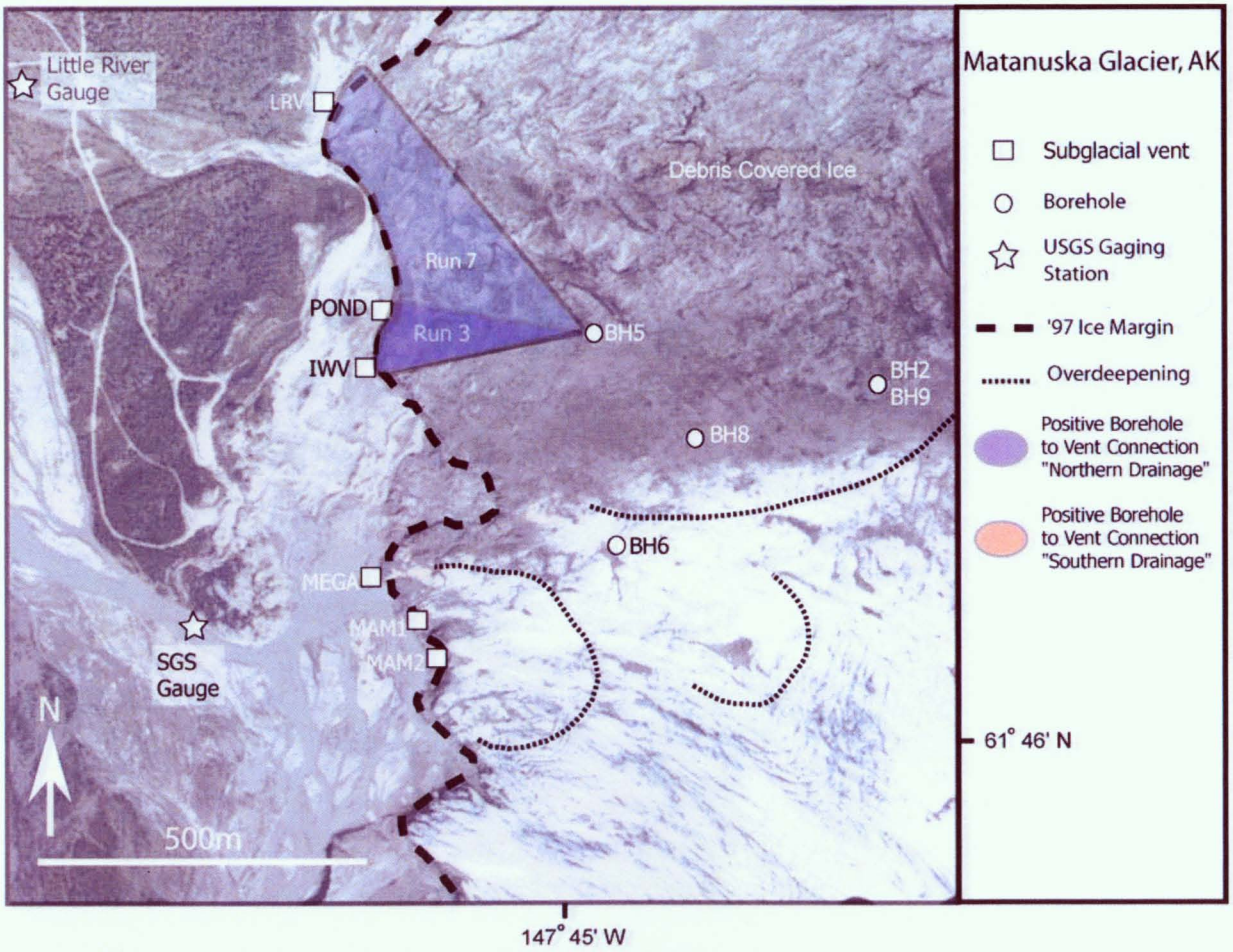

Fig. 23 Borehole to vent connections from experiment run #3 and 7, highlighting expansion of the northern drainage network by the later connection with LRV.

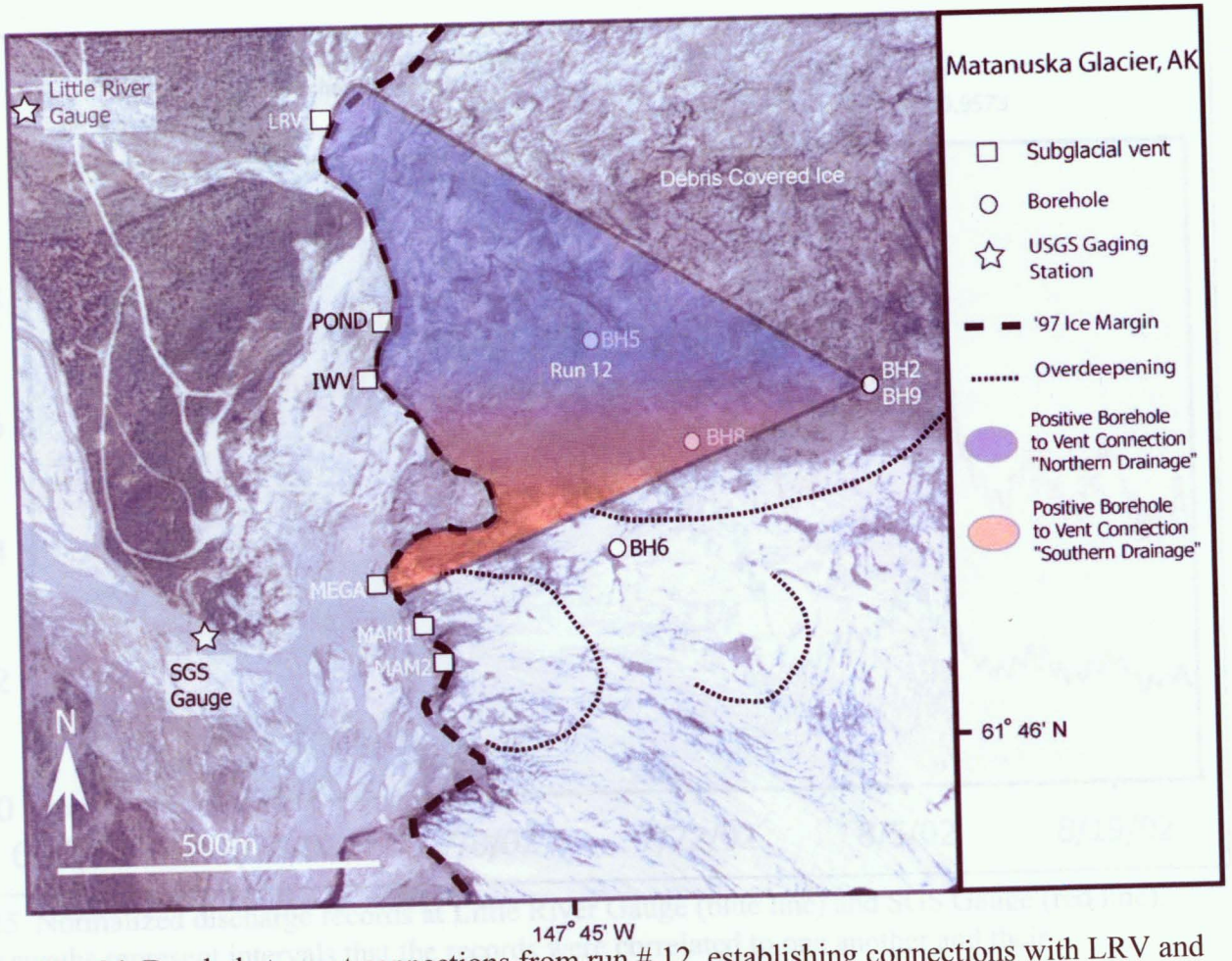

Fig. 24 Borehole to vent connections from run # 12, establishing connections with LRV and MEGA vents separated by ~800m of ice margin. Evidence of a possible expansion and connection of the previously isolated northern and southern drainage systems.

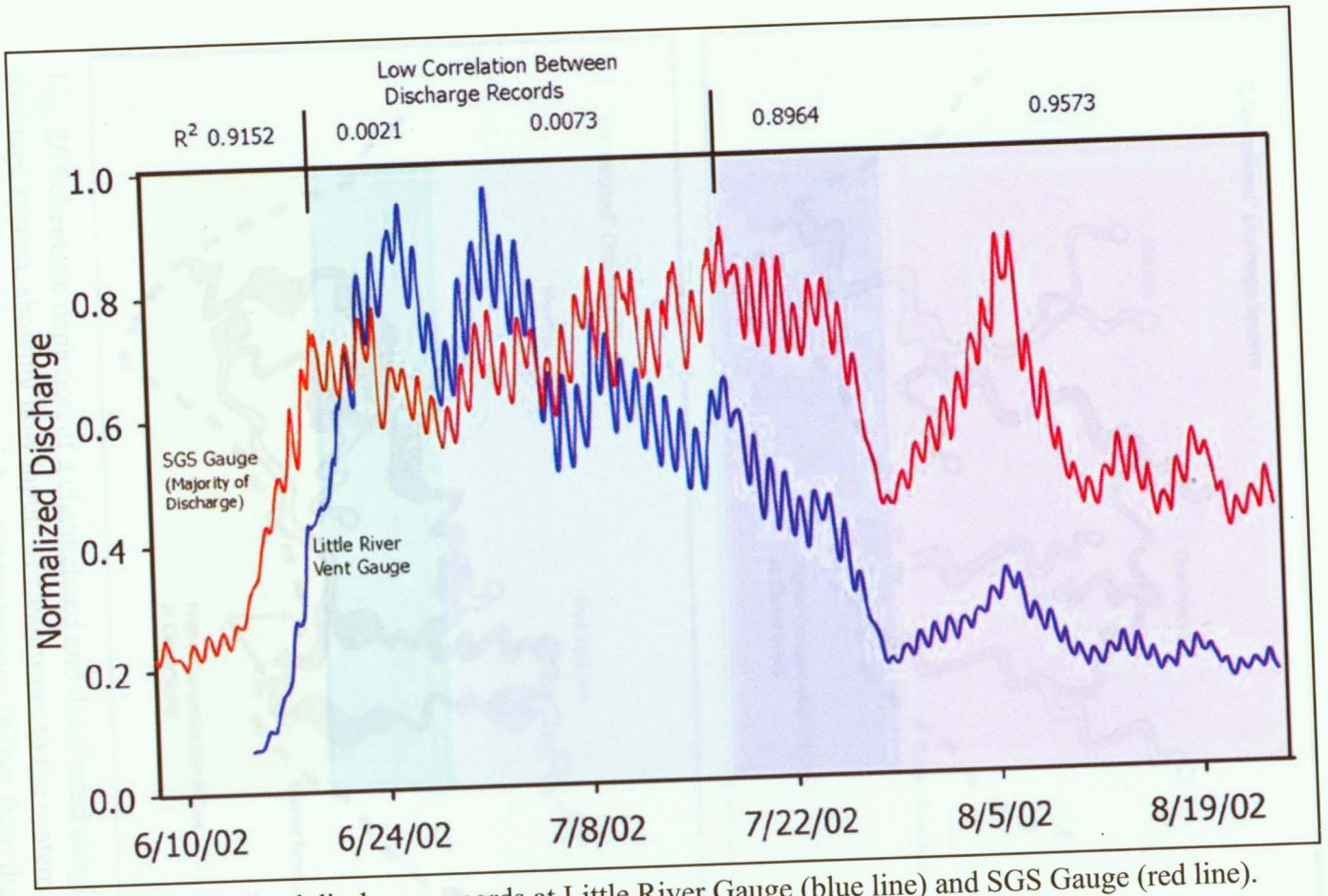

Fig. 25 Normalized discharge records at Little River Gauge (blue line) and SGS Gauge (red line). Color swaths represent intervals that the records were correlated to one another and their corresponding R^2 values.

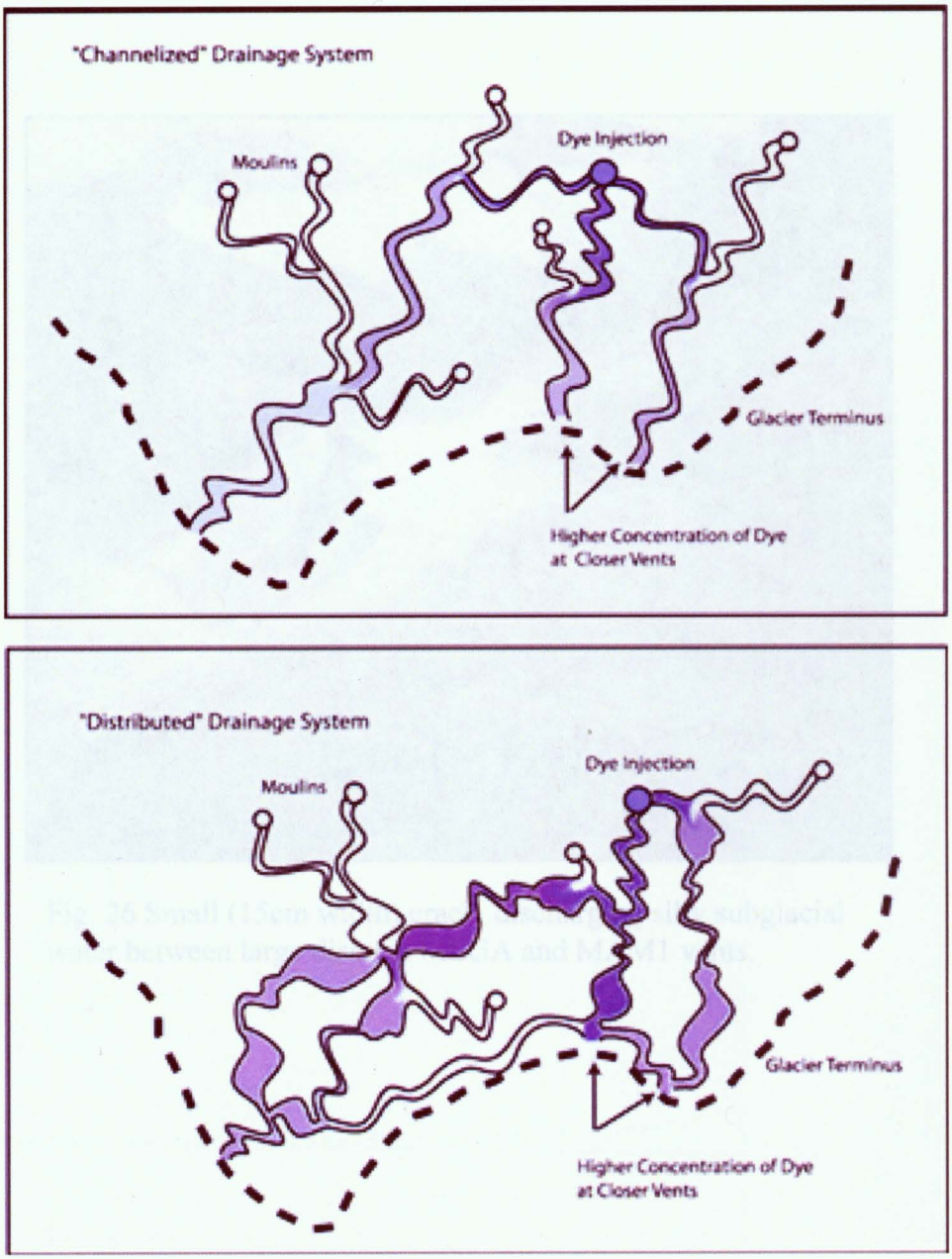

Fig. 26 Schematic depiction of a channelized and distributed subglacial drainage system, showing how inputs of clean water to the system would expect to dilute injected dye concentrations farther from the injections site.

Fig. 26 Small (15cm width) crack, discharging silty subglacial water between large discreet MEGA and MAM1 vents.

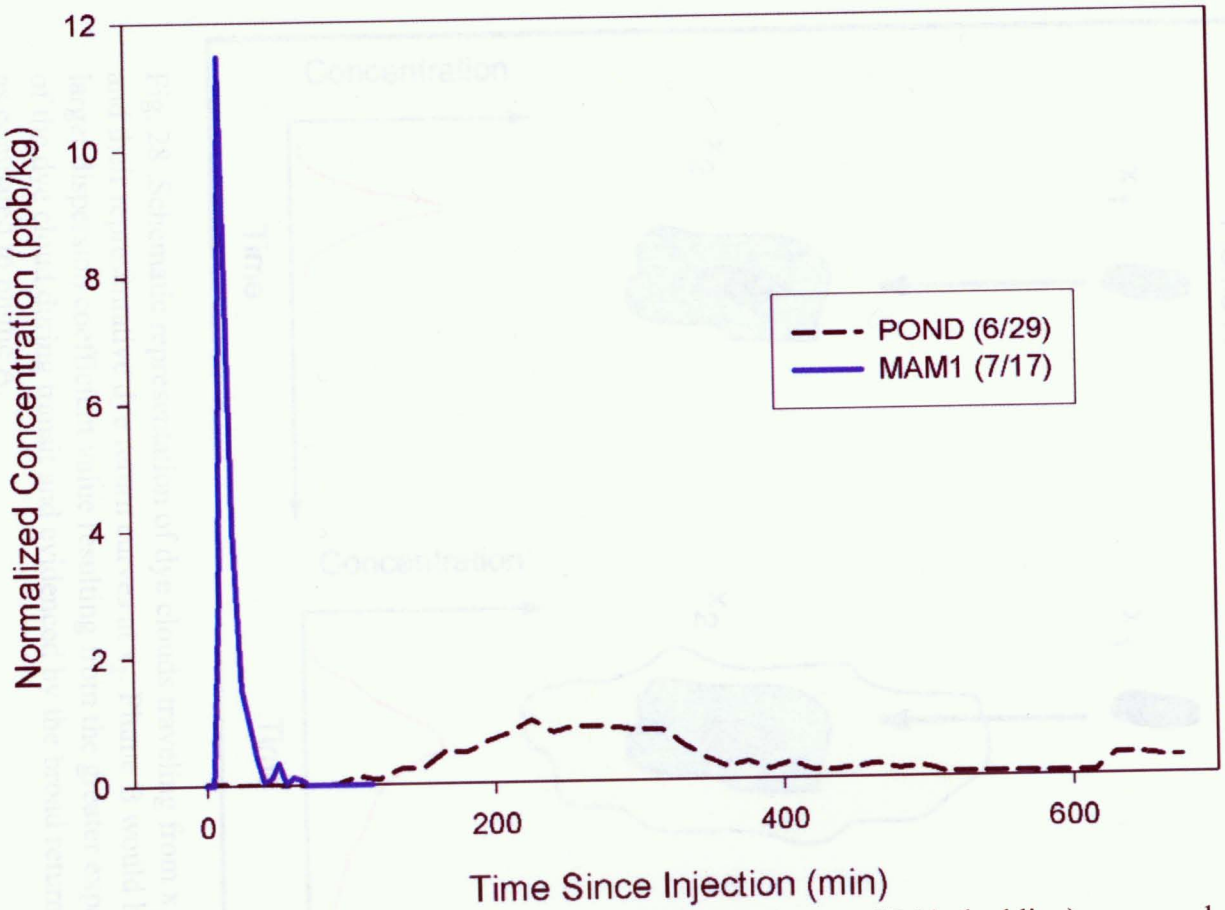

Fig. 27 Dye return curve from BH5 to POND during run #5 (dashed line) compared to the curve from BH6 to MAM1 during run #10 highlighting the qualitative differences within the flowpaths from two similar near terminus injection points.

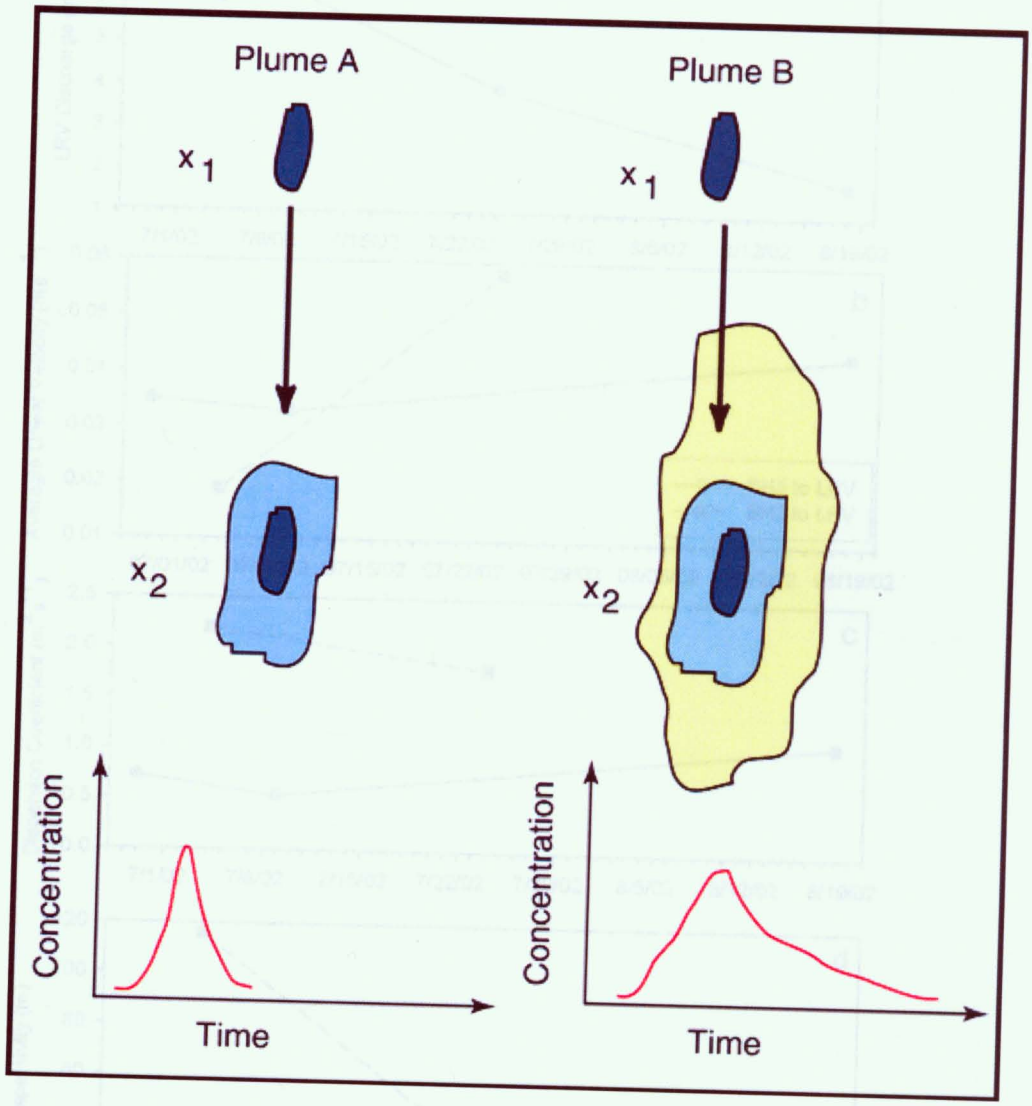

Fig. 28 Schematic representation of dye clouds traveling from x_1 to x_2 and their representative dye return curves at x_2. Plume B would have a larger dispersion coefficient value resulting from the greater expansion of the dye cloud during transit and evidenced by the broad return curve as compared to plume A.

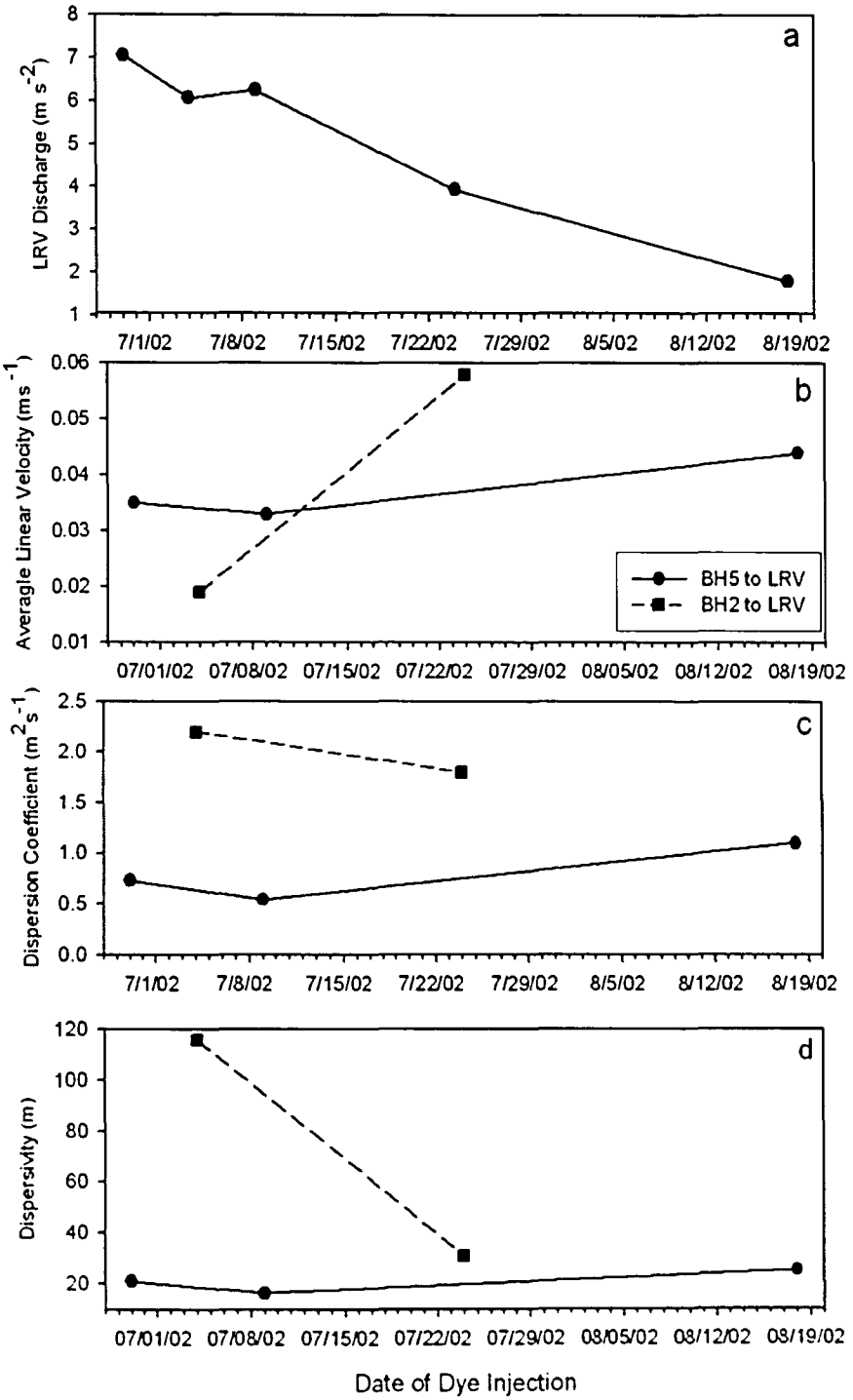

Fig. 29 Plots of a) discharge b) average linear velocity c) dispersion coefficient and d) dispersivity values for BH5 to LRV connections (solid line) and BH2 to LRV (dashed line).

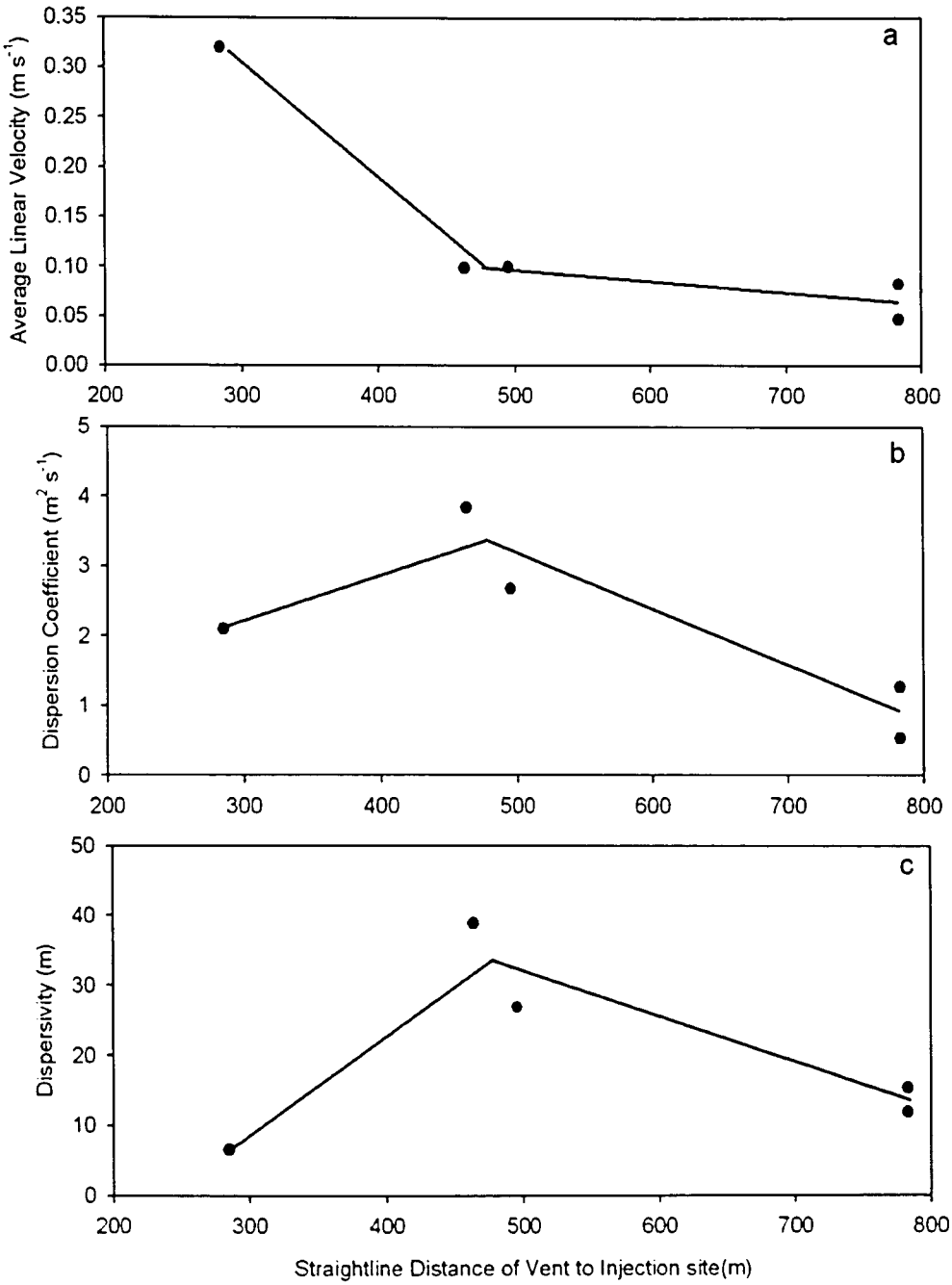

Fig. 30 Plots of a) average linear velocity, b) dispersion coefficient, and c) dispersivity values for MEGA and MAM1 vents from increasing distant BH6, BH8, and BH9 injection points.

8	7/12/02 18:26	BH6, 50m depth 0.9kg injected w/ PVC injector	**Strong**: MEGA (0.216) **Strong**: MAM1 (0.181) **Possible**: LRV (0.041) IWV lost by sediment burial, POND (vent) lost by sediment burial
9	7/16/02 15:16	BH6, surface 0.9kg attempted to air pressure w/PVC injector. Accidental release at surface of borehole.	Bugs not collected, left for repeat test on 7/17.
10	7/17/02 14:30	BH6, 46.1m depth 0.9kg injected w/PVC injector	**Strong**: MEGA (0.343) **Strong**: MAM1 (0.208), **Possible**: IWV(0.027) POND (vent) lost by sediment burial
11	7/21/02 14:15	BH8, 104.9m depth 0.9kg injected w/ PVC injector	**Weak**: MEGA (0.065) **Weak**: MAM1 (0.057) **Possible**: IWV (0.042) **Possible**: MAM2 (0.034, positive connection found with water samples)
12	7/24/02 15:45	BH9 (Original coordinates of BH2), 139m depth 1.36kg injected w/ PVC injector	**Weak**: LRV (0.052) **Weak**: MEGA (0.058) **Possible:** IWV (0.034)
13	8/9/02 13:30	Moulin B, 9m SE of BH8 1.36kg added to surface stream	**Weak**: MEGA (0.062) **Possible**: LRV (0.028)
14	8/18/02 15:20	BH5, now a moulin, 0.9kg. added to surface stream	**Weak :** LRV (0.064) **Possible:** POND (0.034)

Table 1: Summary of tracer injection tests and qualitative connections made between borehole and charcoal bugs in vents. (see Fig. 3 for abbreviations)

Run #	Date/Time (AST)	Injection location, depth of borehole, and test description	Vent Connection Descriptor (measured concentration of dye in elutant, ppb)
1	6/1/02 15:07	BH 2, 107m depth 0.9kg @ 20% solution injected through drill	No connection measured.
2	6/7/02 16:12	BH 2, 107m depth 0.45kg accidental release at surface of borehole, 0.45kg injected at depth through drill	**Possible**: POND (0.041, 0.047 downstream) **Possible:** IWV(0.047)
3	6/9/02 15:21	BH5, 59m depth 0.9kg injected through drill	**Strong**: POND (2.23, 0.899 downstream) **Weak:** IWV (0.877)
4	6/18/02 17:00	Moulin A 4m N of BH2, 0.9kg added to surface stream.	No connection measured.
5	6/29/02 10:27	BH5, 59m depth 0.9kg released from Zip-loc bag	**Strong**: LRV (0.105) **Strong**: POND (0.125, 0.082 downstream) **Strong**: IWV (0.159)
6	7/4/02 15:30	BH2, 104.4m depth 1.25kg injected w/PVC injector	**Possible**: LRV (0.044, positive connection found with water samples) IWV bug lost, screen mesh torn.
7	7/9/02 14:05	BH5, 57.5m depth 0.9kg injected w/ PVC injector	**Strong**: LRV (0.108) **Weak**: POND (0.091, 0.084) **Weak**: IWV(0.079)

Table 1 (contd. on next page)

Run #	Date	Injection site - Outflow Vent	Straight Line Distance (m)	Avg. Discharge Q ($m^3 s^{-1}$)	Dye Recovery (%)	Average Linear Velocity u ($m s^{-1}$)	Dispersion Coefficient D ($m^2 s^{-1}$)	Dispersivity d (m)
3	6/9/02	BH5-POND	250	-	-	0.021	!	!
5	6/29/02	BH5-POND	250	-	-	0.017	0.189	11.1
5	6/29/02	BH5-LRV	538	7.06	90%	0.035	0.73	20.9
6	7/4/02	BH2-LRV	923	6.07	32%	0.019	2.20	115.8
7	7/9/02	BH5-POND	250	-	-	0.014	0.150	10.7
7	7/9/02	BH5-LRV	538	6.26	18%	0.033	0.54	16.4
8	7/12/02	BH6-MEGA	338	-	-	0.38	!	!
8	7/12/02	BH6-MAM1	285	-	-	0.30	!	!
10	7/17/02	BH6-MAM1	285	-	-	0.32	2.10	6.56
11	7/21/02	BH8-MEGA	495	-	-	0.10	2.68	26.8
11	7/21/02	BH8-MAM1	463	-	-	.099	3.84	38.8
11	7/21/02	BH8-MAM2(A)	466	-	-	0.13	8.62	63.4
11	7/21/02	BH8-MAM2 (B)	466	-	-	0.054	0.77	14.3
12	7/24/02	BH9-LRV	919	3.95	5%	0.058	1.80	30.8
12	7/24/02	BH9-MEGA (A)	783	-	-	0.083	1.27	15.3
12	7/24/02	BH9-MEGA (B)	783	-	-	0.047	0.54	11.8
14	8/18/02	BH5-LRV	516	1.80	8%	0.044	1.10	25.1

Table 2. Summary of metrics of flow calculated from dye-breakthrough curves.
! sample rate did not constrain curve sufficiently to capture accurate dispersion parameters.

References

Alley, R.B., Lawson, D.E., Evenson, E.B., Strasser, J.C., and Larson, G.J. 1998, Glaciohydraulic supercooling: A freeze-on mechanism to create stratified, debris-rich basal ice. II. Theory. Journal of Glaciology, 44: 563-569.

Alley, R.B., Strasser, J.C., Lawson, D.E., Evenson, E.B., and Larson, G.J. 1999, Glaciological and geological implications of basal-ice accretion in overdeepenings, *in* Glacial processes past and present, Mickelson, D.M., and Attig, J.W. eds., Geological Society of America, North-Central Section, 31st annual meeting: Madison, WI United States, p. 1-9.

Arconce, S.A., Lawson, D.E., and Delaney, A.J. 1995. Short-pulse radar wavelet recovery and resolution of dielectric contrasts within englacial and basal ice of Matanuska Glacier, Alaska, U.S.A. Journal of Glaciology, 41: 68-86.

Behrens, H., Oerter, H., Reinwarth, O. 1982. Results of tracer experiments with fluorescent dyes on Vernagtferner (Oetztal Alps, Austria) from 1974 to 1982. Zeitschrift fuer Gletscherkunde und Glazialgeologie, 18: 65-83.

Boulton, G.S., Dobbie, K.E. and Zatsepin, S. 2001. Sediment deformation beneath glaciers and its coupling to the subglacial hydraulic system. Quaternary International, 86: 3-28

Brugman, M.M. 1986. Water flow at the base of surging glacier. (Ph.D. thesis) California Institute of Technology, Pasadena, CA.

Burkimsher, M. 1983. Investigations of glacier hydrological systems using dye-tracer techniques: observations at Pasterzengletscher, Austria. Journal of Glaciology, 29: 403-416.

Burnett, B. 2001. Dye tracer experiments on the Matanuska Glacier, AK. (B.S. thesis) Lehigh University, Bethlehem, PA.

Collins, D.N. 1979. Quantitative determination of subglacial hydrology of two alpine glaciers. Journal of Glaciology, 23: 347-361.

Ensminger, S.L., Evenson, E.B., Alley, R.B., Larson, G.J., Lawson, D.E. and Strasser, J.C. 1999. Example of the dependence of ice motion on subglacial drainage evolution: Matanuska Glacier, Alaska, United States. Geological Society of America Special Paper 337: 11-21.

Fountain, A.G. 1993. Geometry and flow conditions of subglacial water at South Cascade Glacier, Washington State, USA; an analysis of tracer injections. Journal of Glaciology, 39: 143-156.

Fountain, A.G. 1994. Borehole water-level variations and implications for the subglacial hydraulics of South Cascade Glacier, Washington State, USA. Journal of Glaciology, 40: 293-304.

Fountain, A.G. and Walder, J.S. 1998. Water flow through temperate glaciers. Reviews of Geophysics, 36: 299-328.

Harbor, J., Sharp, M., Copland, L., Hubbard, B., Nienow, P.W. and Mair, D. 1997. Influence of subglacial drainage conditions on the velocity distribution within a glacier cross-section. Geology, 25: 739-742.

Hasnain, S.I., Jose, P.G., Ahmad, S. and. Negi, D.C. 2001. Character of the subglacial drainage system in the ablation area of Dokriani glacier, India, as revealed by dye-tracer studies. Journal of Hydrology, 248: 216-223.

Hock, R. and Hooke, R.L., 1993. Evolution of the internal drainage system in the lower part of the ablation area of Storglaciaren, Sweden. Geological Society of America Bulletin,105: 537-546.

Hooke, R.L., Miller, S.B., Kohler, J. 1988. Character of the englacial and subglacial drainage system in the upper part of the ablation areas of Storglaciaren, Sweden. Journal of Glaciology, 34: 228-231.

Hooke, R.L. and Pohjola V.A., 1994. Hydrology of a segment of a glacier situated in an overdeepening, Storglaciaren, Sweden. Journal of Glaciology, 40: 140-148.

Hubbard, B.P., Sharp, M.J, Willis, I.C., Nielsen, M.K., Smart, C.C. 1995. Borehole water-level variations and the structure of the subglacial hydrological system of Haut Glacier d'Arolla, Valais, Switzerland. Journal of Glaciology, 41: 572-583.

Hubbard, B.P. and Nienow,P. 1997. Alpine subglacial hydrology. Quaternary ScienceReviews, 16: 939-955.

Kamb, B. 1987. Glacier surge mechanism based on linked cavity configuration of the based water conduit system. Journal of Geophysics Res., 92: 9083-9100.

Kasnavia, T.,Vu, D. and Sabatini D.A. 1999. Fluorescent dye and media properties affecting sorption and tracer selection. Groundwater, 37: 376.

Käss, W. 1998. Tracing Technique in Geohydrology. A.A. Balkema, Rotterdam, Netherlands. pp. 581.

Lawson, D.E., Strasser, J.C., Evenson, E.B. Alley, A.B., Larson, G.L. and Arcone, S.A. 1998. Glaciohydraulic supercooling: a freeze-on mechanism to create stratified, debris-rich, basal ice: I. Field Evidence. Journal of Glaciology, 42: 184-189.

Larsen, 2001. New insight on the character of the hydrologic system of the Matanuska Glacier, Alaska, based on drilling, borehole monitoring, and dye tracing studies. (B.S. Thesis) Carleton College, Northfield, MN.

Milanovic, P. 1981. Karst Hyrdrogeology. Water Resources Publications, Ft. Collins, Colorado. 434 pp.

Mull, D.S., Liberman, T.D., Smoot, J.L. and Woosley, L.H. Jr. 1988. Application of dye-tracing techniques for determining solute-transport characteristics of ground water in karst terrains. USEPA GWPR and USGS WRD. 103 pp.

Nienow, P.W., Sharp, M. and Willis, I.C. 1996. Sampling-rate effects on the properties ofdye breakthrough curves from glaciers. Journal of Glaciology 42: 184-189.

Nienow, P.W., Sharp, M., and Wills, I.C. 1996. Velocity-discharge relationships derived from dye tracer experiments in glacial meltwaters: implications for subglacial flow conditions. Hydrological Processes, 10: 1411-1426.

Nienow P.W., Sharp, M., and Willis I.C. 1998. Seasonal changes in the morphology of the subglacial drainage system, Haut Glacier d'Arolla, Switzerland. Earth Surface Processes and Landforms, 23: 825-843.

Seaberg, S.Z., Seaberg, J.Z., Hooke, R.L. and Wiberg D.W. 1988. Character of the englacial and subglacial drainage system in the lower part of the ablation area of Storglaciaren, Sweden, as revealed by dye-trace studies. Journal of Glaciology, 34: 217-227.

Smart, C.C. 1988. Artificial tracer techniques for the determination of the structure of conduit aquifers. Ground Water, 26: 445-453.

Smart, P.L. and Laidlaw, I.M.S. 1977. An evaluation of some fluorescent dyes for water tracing. Water Resources Research, 13: 15-33.

Theakstone, W. H. and Knudsen, N. T. 1981. Dye tracer tests of water movement at the glacier Austre Okstindbreen, Norway. Norsk Geografisk Tidsskrift, 35: 21-28.

Willis I.C., Sharp, M.J., and Richards, K.S., 1990. Configuration of the drainage system of Midtdalsbreen, Norway, as indicated by dye-tracing experiments. Journal of Glaciology, 36: 89-101.

Wilson, J.F., Cobb, E.D., Kilpatrick, F.A. 1986. Fluorometric procedures for dye tracing. USGS TWRI, Book 3, Chap. A12.

Appendix I.

GPS locations and straight line distances between boreholes and vents

	BH5	Pond	straight line distance (meter)
northing	6849725.207	6849769.65	250.444
easting	460127.652	459881.183	
z	517.234	504.714	

	BH5	LRV	
northing	6849725.207	6850128.239	538.556
easting	460127.652	459770.429	
z	517.234	502.812	

	BH2	Pond	
northing	6849647.879	6849769.65	689.084
easting	460559.423	459881.183	
z	540.461	504.714	

	BH2	LRV	
northing	6849647.879	6850128.239	923.719
easting	460559.423	459770.429	
z	540.461	502.812	

	BH6	MEGA	
northing	6849406.530	6849369.302	337.654
easting	460161.834	459826.239	
z	518.842	496.717	

	BH6	MAM1	
northing	6849406.530	6849310.729	284.820
easting	460161.834	459893.609	
z	518.842	500.467	

	BH8	MEGA	
northing	6849566.861	6849369.302	494.660
easting	460279.735	459826.239	
z	537.519	496.717	

	BH8	MAM1	
northing	6849566.861	6849310.729	463.354
easting	460279.735	459893.609	
z	537.519	497.467	

(continued next page)

	BH8	MAM2	
northing	6849566.861	6849239.365	466.363
easting	460279.735	459947.709	
z	537.519	499.609	

	BH9	BH2	
northing	6849651.332	6849647.879	4.728
easting	460556.194	460559.423	
z	539.719	540.461	

	BH9	MEGA	
northing	6849651.332	6849369.302	782.544
easting	460556.194	459826.239	
z	539.719	496.717	

	BH9	LRV	
northing	6849651.332	6850128.239	919.166
easting	460556.194	459770.429	
z	539.719	502.812	

	BH5a	LRV	
northing	6849735.758	6850128.239	516.586
easting	460106.316	459770.429	
z	517.042	502.812	

Appendix II.

Raw dye concentration data from breakthrough return curves

6/9/02 BH5 to POND Injected @ 15:21ast

Time from Injection (min)	Raw Concentration (ppb)	Normalized Conc. (ppb/kg)
0	0	0.000
10	0	0.000
20	0	0.000
30	0	0.000
40	0	0.000
50	0	0.000
60	0	0.000
70	0	0.000
80	0.008	0.044
90	0.012	0.066
100	0.006	0.033
110	0.103	0.568
120	0.323	1.781
130	0.433	2.387
140	1.12	6.174
150	1.87	10.309
160	2.4	13.230
170	2.18	12.018
180	2.85	15.711
190	3.14	17.310
200	3.28	18.082
210	3.15	17.365
220	3.08	16.979
230	3.06	16.869

6/29/02 BH5 to LRV Injected @ 10:30 ast

Time from Injection (min)	Raw Concentration (ppb)	Normalized Conc. (ppb/kg)	Time from Injection (min)	Raw Concentration (ppb)	Normalized Conc. (ppb/kg)
-30	0.001	0.006	360	0.080	0.441
-15	0.001	0.006	375		0.000
0	0.002	0.011	390	0.079	0.436
15	0.002	0.011	405		0.000
30	0.003	0.017	420	0.060	0.331
45	0.003	0.017	435		0.000
60	0.010	0.055	450	0.088	0.485
75	0.010	0.055	465	0.027	0.149
90	0.000	0.000	480	0.062	0.342
105	0.016	0.088	495	0.026	0.143
120	0.025	0.138	510	0.070	0.386
135	0.080	0.441	525	0.026	0.143
150	0.025	0.138	540	0.058	0.320
165	0.081	0.447	555	0.014	0.077
180	0.099	0.546	570	0.014	0.077
195	0.187	1.031	585	0.012	0.066
210	0.155	0.854	600	0.012	0.066
225	0.192	1.058	615	0.011	0.061
240	0.190	1.047	630	0.011	0.061
255	0.192	1.058	645	0.016	0.088
270	0.196	1.080	660	0.016	0.088
285	0.207	1.141	675	0.008	0.044
300	0.168	0.926			
315	0.145	0.799			
330	0.098	0.540			
345	0.088	0.485			

6/29/02 BH5 to POND Injected @ 10:30 ast

Time from Injection (min)	Raw Concentration (ppb)	Normalized Conc. ppb/kg	Time from Injection (min)	Raw Concentration (ppb)	Normalized Conc. ppb/kg
-30	0.002	0.011	360	0.034	0.187
-15	0.002	0.011	375	0.049	0.270
0	0.003	0.017	390	0.026	0.143
15	0.003	0.017	405	0.045	0.248
30	0.001	0.006	420	0.022	0.121
45	0.001	0.006	435	0.020	0.110
60	0.000	0.000	450	0.029	0.160
75	0.000	0.000	465	0.036	0.198
90	0.001	0.006	480	0.021	0.116
105	0.022	0.121	495	0.031	0.171
120	0.014	0.077	510	0.013	0.072
135	0.042	0.232	525	0.013	0.072
150	0.042	0.232	540	0.013	0.072
165	0.090	0.496	555	0.013	0.072
180	0.086	0.474	570	0.010	0.055
195	0.117	0.645	585	0.010	0.055
210	0.140	0.772	600	0.010	0.055
225	0.175	0.965	615	0.010	0.055
240	0.139	0.766	630	0.060	0.331
255	0.154	0.849	645	0.060	0.331
270	0.156	0.860	660	0.050	0.276
285	0.147	0.810	675	0.050	0.276
300	0.144	0.794			
315	0.142	0.783			
330	0.099	0.546			
345	0.063	0.347			

7/4/02 BH2 to LRV injected @ 15:30 ast

Time from Injection (min)	Raw Concentration (ppb)	Normalized Conc. (ppb/kg)
0	0	0.000
45	0.003	0.012
90	0.003	0.012
135	0	0.000
180	0.008	0.032
225	0.012	0.048
270	0.01	0.040
315	0.013	0.052
360	0.01	0.040
405	0.017	0.068
450	0.021	0.084
495	0.03	0.120
540	0.033	0.132
585		
630		
675	0.019	0.076
720	0.025	0.100
765	0.023	0.092
810	0.025	0.100
855	0.031	0.124
900	0.02	0.080
945	0.022	0.088
990	0.024	0.096
1035	0.024	0.096
1080	0.014	0.056
1125	0.023	0.092
1170	0.017	0.068
1215	0.018	0.072
1260	0.022	0.088
1305	0.01	0.040
1350	0.012	0.048
1395	0.012	0.048
1440	0.006	0.024
1485	0.006	0.024
1530	0.003	0.012
1575	0.006	0.024

7/9/02 BH5 to LRV injected @ 14:05 as
t

Time from Injection (min)	Raw Concentration (ppb)	Normalized Conc. (ppb/kg)	Time from Injection (min)	Raw Concentration (ppb)	Normalized Conc. (ppb/kg)
-5	0		550	0	0.000
10	0	0.000	565	0	0.000
25	0.014	0.077	580	0	0.000
40	0	0.000	595	0	0.000
55	0	0.000	610	0	0.000
70	0	0.000	625	0	0.000
85	0	0.000	640	0	0.000
100	0	0.000	655	0	0.000
115	0.005	0.028			
130	0	0.000			
145	0.006	0.033			
160	0.008	0.044			
175	0.013	0.072			
190	0.022	0.121			
205	0.023	0.127			
220	0.023	0.127			
235	0.03	0.165			
250	0.029	0.160			
265	0.049	0.270			
280	0.04	0.221			
295	0.038	0.209			
310	0.025	0.138			
325	0.037	0.204			
340	0.03	0.165			
355	0.019	0.105			
370	0.008	0.044			
385	0.019	0.105			
400	0.019	0.105			
415	0.024	0.132			
430	0.017	0.094			
445	0.008	0.044			
460	0.019	0.105			
475	0.02	0.110			
490	0.007	0.039			
505	0.009	0.050			
520	0	0.000			
535	0.004	0.022			

7/9/02 BH5 to POND injected @ 14:05 ast

Time from Injection (min)	Raw Concentration (ppb)	Normalized Conc. (ppb/kg)	Time from Injection (min)	Raw Concentration (ppb)	Normalized Conc. (ppb/kg)
-5	0	0.000	550	0.002	0.011
10	0	0.000	565	0.003	0.017
25	0	0.000	580	0	0.000
40	0.003	0.017	595	0	0.000
55	0.028	0.154	610	0	0.000
70	0.004	0.022	625	0.002	0.011
85	0.006	0.033	640	0	0.000
100	0.007	0.039	655	0	0.000
115	0.006	0.033			
130	0.01	0.055			
145	0.02	0.110			
160	0.007	0.039			
175	0.025	0.138			
190	0.021	0.116			
205	0.029	0.160			
220	0.038	0.209			
235	0.053	0.292			
250	0.054	0.298			
265	0.063	0.347			
280	0.046	0.254			
295	0.053	0.292			
310	0.04	0.221			
325	0.056	0.309			
340	0.042	0.232			
355	0.039	0.215			
370	0.037	0.204			
385	0.029	0.160			
400	0.035	0.193			
415	0.029	0.160			
430	0.01	0.055			
445	0.02	0.110			
460	0.006	0.033			
475	0.017	0.094			
490	0.013	0.072			
505	0.013	0.072			
520	0.011	0.061			
535	0.003	0.017			

7/12/02 BH6 to MEGA
injected @ 18:26 AST

Time from Injection (min)	Raw Concentration (ppb)	Normalized Conc. (ppb/kg)
0	0	0
15	0.556	3.065
30	0.086	0.474
45	0.055	0.303
60	0.005	0.028
75	0.027	0.149
90	0	0
105	0	0
120	0	0
135	0	0
150	0	0
165	0	0
180	0	0
195	0	
210	0	
225	0	
240	0	
255	0	
270	0	
285	0	
300	0	
315	0	
330	0	
345	0	

7/12/02 BH6 to MAM1
injected @ 18:26 AST

Time from Injection (min)	Raw Concentration (ppb)	Normalized Conc. (ppb/kg)
0	0	0
15	1.5	8.269
30	0.565	3.115
45	0.126	0.695
60	0.043	0.237
75	0.05	0.276
90	0.007	0.039
105	0.035	0.193
120	0	0.000
135	0.004	0.022
150	0	0
165	0	0
180	0	0
195	0	
210	0	
225	0	
240	0	
255	0	
270	0	
285	0	
300	0	
315	0	
330	0	
345	0	

7/17/02 BH6 to MAM1 injected @ 14:30 AST

Time from Injection (min)	Raw Concentration (ppb)	Normalized Conc. (ppb/kg)
0	0	0.000
5	0	0.000
10	0.535	2.949
15	2.08	11.466
20	0.729	4.019
25	0.272	1.499
30	0.177	0.976
35	0.077	0.424
40	0.007	0.039
45	0.017	0.094
50	0.061	0.336
55	0.004	0.022
60	0.02	0.110
65	0.015	0.083
70	0	0
75	0	0
80	0	0
85	0	0
90	0	0
95	0	0
100	0	0
105	0	0
110	0	0
115	0	0

7/21/02 BH8 to MEGA
injected @ 14:00 AST

Time from Injection (min)	Raw Concentration (ppb)	Normalized Conc. (ppb/kg)
15	0	0.000
30	0.002	0.011
45	0	0.000
60	0.04	0.221
75	0.042	0.232
90	0.049	0.270
105	0.022	0.121
120	0.026	0.143
135	0.008	0.044
150	0.023	0.127
165	0.012	0.066
180	0.01	0.055
195	0	0.000
210	0.01	0.055
225	0	0
240	0	0
255	0	0
270	0	0
285	0	0
300	0	0
315	0	0
330	0	0
345	0	0
360	0	0

7/21/02 BH8 to MAM1
injected @ 14:00AST

Time from Injection (min)	Raw Concentration (ppb)	Normalized Conc. (ppb/kg)
15	0	0
30	0.003	0.017
45	0.025	0.138
60	0.077	0.424
75	0.062	0.342
90	0.06	0.331
105	0.03	0.165
120	0.049	0.270
135	0.004	0.022
150	0.01	0.055
165	0.009	0.050
180	0.005	0.028
195	0.006	0.033
210	0.006	0.033
225	0	0.000
240	0	0
255	0	0
270	0	0
285	0	0
300	0	0
315	0	0
330	0	0
345	0	0
360	0	0

7/21/02 BH8 to MAM2 injected @ 14:00 AST

Time from Injection (min)	Raw Concentration (ppb)	Normalized Conc. (ppb/kg)
15	0	0
30	0.023	0.127
45	0.043	0.237
60	0.028	0.154
75	0.017	0.094
90	0.019	0.105
105	0.011	0.061
120	0.031	0.171
135	0.021	0.116
150	0.032	0.176
165	0.036	0.198
180	0.018	0.099
195	0.011	0.061
210	0.007	0.039
225	0.019	0.105
240	0.002	0.011
255	0	0
270	0	0
285	0	0
300	0	0
315	0	0
330	0	0
345	0	0
360	0	0

7/24/02 BH9 to MEGA
injected @ 15:45 AST

Time from Injection (min)	Raw Concentration (ppb)	Normalized Conc. (ppb/kg)
45	0	0
60	0	0
75	0	0
90	0	0
105	0	0
120	0.013	0.048
135	0.024	0.088
150	0.032	0.118
165	0.015	0.055
180	0.016	0.059
195	0.017	0.062
210	0.007	0.026
225	0.001	0.004
240	0.005	0.018
255	0.015	0.055
270	0.006	0.022
285	0.02	0.073
300	0.014	0.051
315	0.01	0.037
330	0.004	0.015
345	0.006	0.022
360	0	0
375	0	0
390	0	0
405	0	0
420	0	0
435	0	0
450	0	0
465	0	0
480	0	0
495	0	0
510	0	0
525	0	0

7/24/02 BH9 to LRV
injected @ 15:45 AST

Time from Injection (min)	Raw Concentration (ppb)	Normalized Conc. (ppb/kg)
45	0	0
60	0	0
75	0	0
90	0	0
105	0	0
120	0	0
135	0	0
150	0	0
165	0.011	0.040
180	0	0.000
195	0.028	0.103
210	0.035	0.129
225	0.027	0.099
240	0.041	0.151
255	0.029	0.107
270	0.03	0.110
285	0.032	0.118
300	0.028	0.103
315	0.035	0.129
330	0.027	0.099
345	0.014	0.051
360	0.009	0.033
375	0.01	0.037
390	0.01	0.037
405	0.01	0.037
420	0.005	0.018
435	0	0.000
450	0.004	0.015
465	0	0
480	0	0
495	0	0
510	0	
525	0	

8/18/02 BH5 to LRV injected @ 14:00 AST

Time from Injection (min)	Raw Concentration (ppb)	Normalized Conc. (ppb/kg)
30	0	0.000
60	0.012	0.066
90	0	0.000
120	0.016	0.088
150	0.068	0.375
180	0.057	0.314
210	0.036	0.198
240	0.032	0.176
270	0.046	0.254
300	0.018	0.099
330	0.02	0.110
360	0.023	0.127
390	0.026	0.143
420	0.022	0.121
450	0.014	0.077
480	0.022	0.121
510	0.006	0.033
540	0	0.000
570	0.008	0.044
600	0	0.000
630	0	0.000
660	0	0.000
690	0	0.000
720	0	0.000

Vita

James Joseph Cascione son of Stephen and Olga Cascione was born in S. Setauket, NY spending most of his childhood collecting stones from the beach. James graduated from Ward Melville High School in 1998. He then earned a B.S. in Earth and Environmental Sciences from Lehigh University in 2002. He was accepted into the graduate program later that same year. While at Lehigh James was both a T.A. and R.A. within the department, including spending three summers with Lehigh University's Geology Field Camp.

END OF TITLE